ผลของแบเรียมออกไซด์ต่อลักษณะเฉพาะวาริสเตอร์ของสารเซรามิกซิงค์ออกไซด์

นางสาว จิราภรณ์ เอื้อชลิตานุกูล

วิทยานิพนธ์นี้เป็นส่วนหนึ่งของการศึกษาตามหลักสูตรปริญญาวิทยาศาสตรมหาบัณฑิต

สาขาวิชาเทคโนโลยีเซรามิก ภาควิชาภาควิชาวัสดุศาสตร์

คณะวิทยาศาสตร์ จุฬาลงกรณ์มหาวิทยาลัย

ปีการศึกษา 2543

ISBN 974-346-714-9

EFFECT OF BARIUM OXIDE ON THE VARISTOR CHARACTERISTICS OF ZINC OXIDE CERAMICS

Miss Chiraporn Auechalitanukul

A Thesis Submitted in Partial Fulfillment of the Requirements
for the Degree of Master of Science in Ceramic Technology

Department of Materials Science
Faculty of Science
Chulalongkorn University

Academic Year 2000
ISBN 974-346-714-9

Thesis Title	EFFECT OF BARIUM OXIDE ON THE VARISTOR CHARACTERISTICS OF ZINC OXIDE CERAMICS
By	Chiraporn Auechalitanukul
Department	Materials Science
Thesis Advisor	Assistant Professor Sutin Kuharuangrong, Ph.D.
Thesis Co-advisor	

Accepted by the Faculty of Science, Chulalongkorn University in Partial Fulfillment of the Requirements for the Master 's Degree

…….. Dean of Faculty of Science

(Associate Professor Wanchai Phothiphichitr, Ph.D.)

THESIS COMMITTEE

…….. Chairman

(Associate Professor Khemchai Hemachandra, Ph.D.)

……. Thesis Advisor

(Assistant Professor Sutin Kuharuangrong, Ph.D.)

…….. Member

(Associate Professor Supatra Jinawath, Ph.D.)

…….. Member

(Sirithan Jiemsirilers, Ph.D.)

…….. Member

(Pavadee Aungkavattana, Ph.D.)

จิราภรณ์ เอื้อชลิตานุกูล : ผลของแบเรียมออกไซด์ต่อลักษณะเฉพาะวาริสเตอร์ของสารเซรามิกซิงค์ออกไซด์. (EFFECT OF BARIUM OXIDE ON THE VARISTOR CHARACTERISTICS OF ZINC OXIDE CERAMICS) อ. ที่ปรึกษา : ผศ. ดร. สุทิน คูหาเรืองรอง, 66 หน้า. ISBN 974-346-714-9.

ซิงค์ออกไซด์วาริสเตอร์มีลักษณะของความสัมพันธ์ระหว่างกระแสไฟฟ้าและศักย์ไฟฟ้าที่ไม่เป็นเส้นตรง ทำให้สามารถนำไปใช้งานเป็นตัวป้องกันความเสียหายของวงจรไฟฟ้าจากศักย์ไฟฟ้าที่สูงเกินได้ ความไม่เป็นเส้นตรงสามารถพบได้ในซิงค์ออกไซด์ที่มีตัวเติมบางชนิดผสมอยู่ เช่น บิสมัธออกไซด์ แบเรียมออกไซด์ และอื่นๆ งานวิจัยนี้ได้ศึกษาผลของแบเรียม (0.5 และ 1 เปอร์เซ็นต์โดยน้ำหนัก) ต่อเฟส โครงสร้างจุลภาค และลักษณะเฉพาะระหว่างกระแสไฟฟ้าและศักย์ไฟฟ้าของสารเซรามิกซิงค์ออกไซด์ที่มีบิสมัธผสมอยู่ 5 เปอร์เซ็นต์โดยน้ำหนัก นอกจากนี้ยังมีการเปรียบเทียบค่าสัมประสิทธิ์ของความไม่เป็นเส้นตรงและโครงสร้างจุลภาคระหว่างการเผาอบผนึกที่อุณหภูมิ 900 องศาเซลเซียสและ 1000 องศาเซลเซียส

จากผลการวิเคราะห์ด้วยเครื่องเอ็กซ์เรย์ดิฟแฟรกโตมิเตอร์แสดงให้เห็นว่าแบเรียมออกไซด์สามารถป้องกันการระเหยของบิสมัธซึ่งประพฤติตัวเสมือนชั้นฉนวนไฟฟ้าของเกรน ค่าสัมประสิทธิ์ของความไม่เป็นเส้นตรงจึงมีค่าสูงขึ้นในตัวอย่างที่เติมด้วยแบเรียม แบเรียมออกไซด์ยังเพิ่มขนาดของเกรนซึ่งส่งผลให้ค่าสัมประสิทธิ์ของความไม่เป็นเส้นตรงเพิ่มขึ้น แต่อย่างไรก็ตามการมีแบเรียมออกไซด์ทำให้จำเป็นต้องใช้อุณหภูมิในการเผาอบผนึกเพิ่มขึ้นเพื่อให้ได้ความหนาแน่นที่เหมาะสม สำหรับการเผาอบผนึกที่อุณหภูมิ 1000 องศาเซลเซียสจะทำให้ได้ค่าสัมประสิทธิ์ของความไม่เป็นเส้นตรงสูงกว่าการเผาอบผนึกที่อุณหภูมิ 900 องศาเซลเซียส และยังทำให้ได้โครงสร้างจุลภาคที่สม่ำเสมอกว่าด้วย

ภาควิชา วัสดุศาสตร์	ลายมือชื่อนิสิต .....
สาขาวิชา เทคโนโลยีเซรามิก	ลายมือชื่ออาจารย์ที่ปรึกษา .....
ปีการศึกษา 2543	ลายมือชื่ออาจารย์ที่ปรึกษาร่วม .....

4172255823 : MAJOR CERAMIC TECHNOLOGY

KEY WORD: VARISTOR / ZINC OXIDE / NONLINEAR CHARACTERISTIC / BISMUTH OXIDE / BARIUM OXIDE

CHIRAPORN AUECHALITANUKUL : EFFECT OF BARIUM OXIDE ON THE VARISTOR CHARACTERISTICS OF ZINC OXIDE CERAMICS.

THESIS ADVISOR : ASSIST. PROF. SUTIN KUHARUANGRONG, Ph.D. 66 pp.

ISBN 974-346-714-9.

Zinc oxide (ZnO) varistors can be used as the overvoltage surge protectors in the electronic circuit because of their nonlinear current-voltage (I-V) characteristic. This property can be observed in ZnO containing other additives such as bismuth oxide, barium oxide, etc. In this research, the effects of 0.5 and 1.0 wt% BaO on the phase, microstructure and I-V characteristic of 95 wt% ZnO - 5 wt% Bi_2O_3 were investigated. Furthermore, sintering at 900°C and 1000°C were compared, especially, on the nonlinear coefficient and microstructure of those compositions.

The results from XRD showed that BaO could prevent the evaporation of Bi_2O_3 acted as an insulating layer of grains. Consequently, a higher nonlinear coefficient was obtained from 95 wt% ZnO - 5 wt% Bi_2O_3 doped with Ba. In addition, BaO increased the grain size of this composition affecting a higher nonlinear coefficient. However, the higher sintering temperature was required to maintain the optimum density of sample. Moreover, the compositions sintered at 1000°C provided not only a higher value of the coefficient but also uniform microstructure than those sintered at 900°C.

Department Materials Science — Student's signature……

Field of study Ceramic Technology — Advisor's signature……

Academic year 2000 — Co-advisor's signature……

ACKNOWLEDGEMENTS

I would like to express my deep gratitude to my advisor, Assistant Professor Dr. Sutin Kuharuangrong for her useful help, advice and guidance throughout the course of this task. I am grateful to Dr. Pavadee Angkavattana and Dr. Chutima Eamchotchawalit for their kind helps. I also sincerely thank to my thesis committee for their suggestions.

I gratefully acknowledge the thesis support from the Graduate School of Chulalongkorn University for financial support and the National Metal and Materials Technology Center (MTEC) and the Department of Materials Science, Faculty of Science, Chulalongkorn University, for the research facilities.

My appreciation are also extended to my good friends for friendships and Mr. Wichit Prakaypun for his encouragement and help.

Finally, I am very much indebted to my family for their love, encouragement and worthy moral support though my life.

CONTENTS

Chapter Page

LIST OF TABLES

Table Page

LIST OF FIGURES

Figure Page

LIST OF FIGURES

Figure Page

Figure Page

Figure Page

Figure Page

CHAPTER 1
INTRODUCTION

At present, an electronic circuit has been utilized in most of equipments and instruments. However, it can be destroyed by the overvoltage. To protect the apparatus, an energy limiting device must be installed. Fuse is usually used as a barrier to limit the current and voltage. Under normal conditions, the device is passive and allows the apparatus to function properly. Under fault conditions, the fuse will blow to prevent the circuit from burning or allowing the excess voltage and current to reach the devices.

In addition to the fuse, the varistor, another type of intrinsic safety barrier, can also arrest the surges. Unlike the fuses, it can protect the circuits from the overvoltage without destroying itself. Therefore, it can be reused for several times. In other words, the replacement of the suppressors is not required for a long period of time.

Varistors can be produced from semiconducting materials such as silicon carbide (SiC), zinc oxide (ZnO), titanium dioxide (TiO_2) and strontium titanate ($SrTiO_3$) with suitable dopants. ZnO is widely used as the commercial composition and has been extensively studied for many years. It normally contains some additives that are metal oxide compounds. These dopants can improve the electrical properties of ZnO and usually obtained when the multiple dopants are used. Bismuth oxide (Bi_2O_3) and barium oxide (BaO) are the most common additives and used with other metal oxide dopants. However, these two oxides affecting the properties of ZnO have not been clearly identified.

In this thesis, the effect of BaO on the varistor characteristics of Bi_2O_3-doped ZnO ceramics was studied. Moreover, the microstructure related to the electrical properties and the sintering temperature of these compositions was determined.

CHAPTER 2
LITERATURE REVIEW

2.1 Introduction

The varistors are electronic ceramic devices with highly nonlinear current-voltage (I-V) characteristics enabling them to be used as reversible, solid-state switches with large energy absorption capabilities. Functionally, they can limit the overvoltage equally in both polarities that are similar to back-to-back diodes without being destroyed. They are typically used in parallel with electronic circuits in both the ac- and dc- fields to protect them from voltage surges ranging from a few volts to tens of kilovolts.

The original varistor ceramics were firstly developed in the early 1930s for protecting telephone systems instead of selenium rectifiers. Silicon carbide (SiC) varistors were developed by the Bell System. After their successive improvements in processing taken place both in the United States and Japan, the ZnO varistor has been extensively developed in Japan since 1969.

The ZnO-based varistor is prepared by mixing powder of ZnO with small amounts of additives such as bismuth, antimony, cobalt, etc., forming this mixed powder and sintering it. The resultant product is comprised of the conductive ZnO grains and the resistive grain boundaries. The unique grain boundary property contributes to the good nonlinear I-V characteristics.

In addition to its highly nonlinear I-V characteristic, the range of voltage and current over which the device can be used and also the range of energy absorption capability are far superior to those of SiC-based device. This versatility can provide varistors to be useful both in the semiconductor industry as well as in the power industry.

2.2 Fundamental Characteristics of Zinc Oxide Varistors

2.2.1 Electrical Properties of Zinc Oxide Varistors

The most important property of the ZnO varistors is the nonlinear I-V characteristic as illustrated in Figure 2.1[1]. The logarithmic I-V characteristic is typically represented, since the current and voltage vary over so many orders of magnitude. At low voltages, in prebreakdown region, the linear I-V relation occurs, but above a certain voltage, called breakdown or threshold voltage, the current varies with voltage and the relation between them is nonlinear. In this nonlinear region, the expression, given as power-law, obeys the equation (2.1).

$$I \propto V^{\alpha} \tag{2.1}$$

The exponent (α), usually called nonlinear coefficient, is a measure of how rapidly current increases with applied voltage and is often used as a figure of merit. It is defined by the equation (2.2).

$$\alpha = \frac{d\ln(I)}{d\ln(V)} \tag{2.2}$$

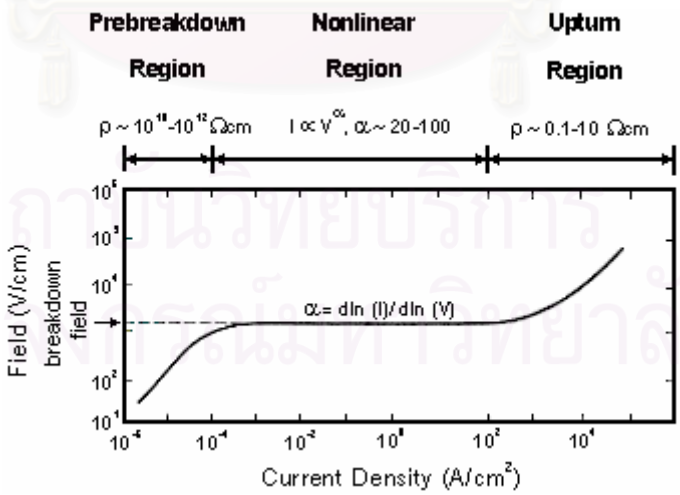

Figure 2.1 Nonlinear current-voltage characteristic of a ZnO-based varistor[1].

The nonlinearity can be very large, with a coefficient of 30-80 for many commercial varistors. Therefore, the current can be vary by orders of magnitude with

only small changes in voltage. At still higher voltages (upturn region), a second linear (ohmic) regime occurs. Unlike dielectric breakdown, varistor has a reversible breakdown (with no or little hysteresis), and upon decreasing voltage below the breakdown voltage, it becomes ohmic again. However, the degradation can result if a varistor is held in the breakdown or nonlinear region and large amounts of resistive self-heating are allowed to occur.

Functionally, the varistor can be regarded as a resistor prior to reaching the breakdown voltage and as a conductor thereafter. At the steady operating voltage, it is in the resistive state with low leakage current. When the voltage exceeds the breakdown voltage, for instance, the varistor becomes high conducting and shunts the voltage through it to ground before the apparatus is damaged. Finally, when the voltage returns to normal, the varistor returns to the resistive state.

The breakdown voltage, also called nonlinear voltage, increases linearly as the varistor thickness increases, and it decreases linearly as the average grain size of the ZnO grains decreases. An increase in the sintering temperature, enhancing the ZnO grain growth, results in a decrease of the nonlinear voltage[2,3]. From these facts, it is suggested that the nonlinear behavior of varistor is associated with the grain boundaries. The model constructed (Figure 2.2) is used to calculate the electrical properties of the individual grain boundaries[4]. The properties calculated are in good agreement with measured values. For example, if "t" is thickness of the sample and "$\bar{d}$" is the average diameter of the ZnO grains, then "s", the number of junctions along the thickness of sample, is estimated from the equation (2.3).

$$s = \frac{t}{\bar{d}} \tag{2.3}$$

"V" calculated from the equation (2.4) is the voltage across a single grain boundary when the applied voltage is equal to the breakdown voltage nominated by V_{1mA} (V_{1mA} represented the voltage at the current of 1 mA). The accuracy of these

calculations is not, of course, very high because, in reality, the average grain size is a statistical parameter[5].

$$V = \frac{V_{1mA}\,\bar{d}}{t} \tag{2.4}$$

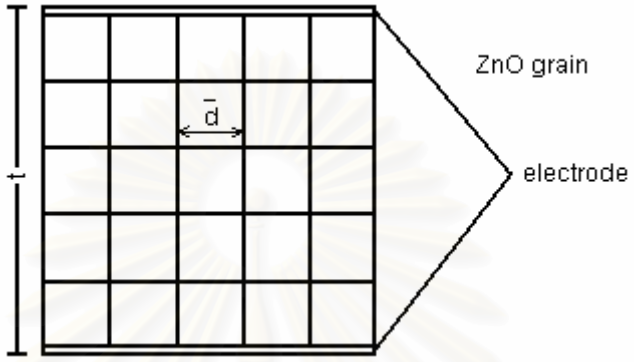

Figure 2.2 Structural model of a varistor material with cubic ZnO grains[4].

The current-voltage characteristic also varies with temperature in the way presented in Figure 2.3[6]. In prebreakdown region, the effect of temperature is relatively strong and the current quickly increases with increasing temperature. In contrast, the temperature unaffects on this characteristic in nonlinear and upturn regions, e.g. V at a current of 1 mA only slightly decreases with temperature. Hence, it can infer that the carrier transport mechanisms, predominating in each region differ from one another.

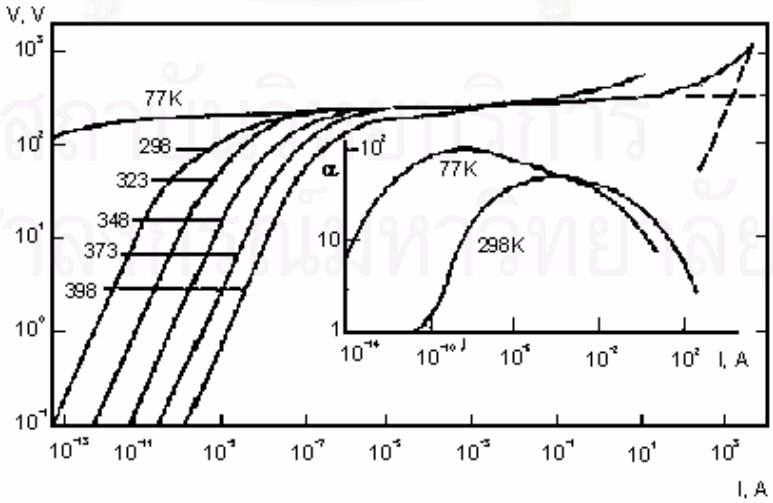

Figure 2.3 Variation of the current-voltage characteristic as a function of temperature of a ZnO varistor[6].

The I-V characteristic of a varistor depends on the factor involved in the fabrication. These nonlinear characteristics are found only when sintering process is carried out in air or oxygen[7]. A reduction in oxygen partial pressure leads to an increase in the leakage current, corresponding to a decrease of the nonlinear coefficient (α). In Matsuoka's work[7], the nonlinear coefficient reaches a maximum when this content is a few percent (Figure 2.4), although the V_{1mA} increases with increasing content of additives. As previously mentioned, the voltage V_{1mA} also depends on the sintering temperature, therefore the varistor properties can be improved by controlling the process parameters. As a result, the different types and different nominal voltages can be produced by using the same chemical composition and fabricating pellets of the same thickness. This is significant because the ability of a varistor to absorb the energy of a current surge depends on its volume.

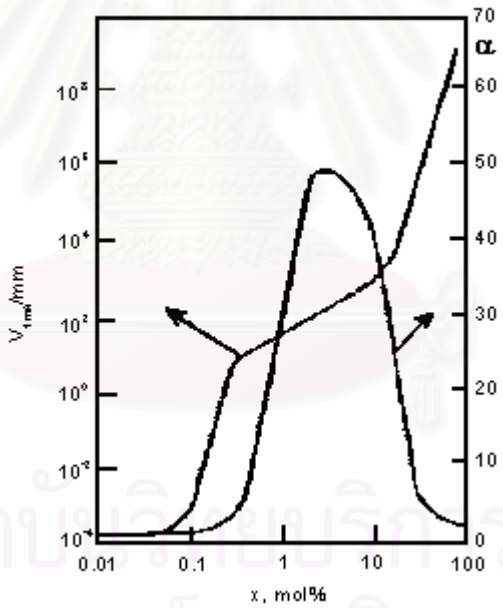

Figure 2.4 Variations of V_{1mA} and nonlinear coefficient (α) as functions of the total content of additives (x); x - the total content of Bi_2O_3, Sb_2O_3, CoO, MnO_2, and Cr_2O_3 (1:2:1:1:1)[7].

Figure 2.5 displays how an addition of various metal oxides affects the I-V characteristic of a varistor. It is believed that a Bi_2O_3 addition results in the nonlinear behavior. Other suggestion is that the same role may be played by oxide of other metals of large in radius, such as rare earth metal[8-10] or barium[11,12]. Small ion radius

metal oxides, such as Mn and Co, diffuse into the ZnO grains and also give a rise of the nonlinearity. They also affect the conductivity of the ZnO. The I-V characteristic shifts towards greatly current density. The shape of the curve with upturn region depends on the oxide content of trivalent metals of small ion radius, such as Al and Ga[13]. The amount of the latter additives should not exceed 50-150 ppm, since the great increase in the leakage current occurs.

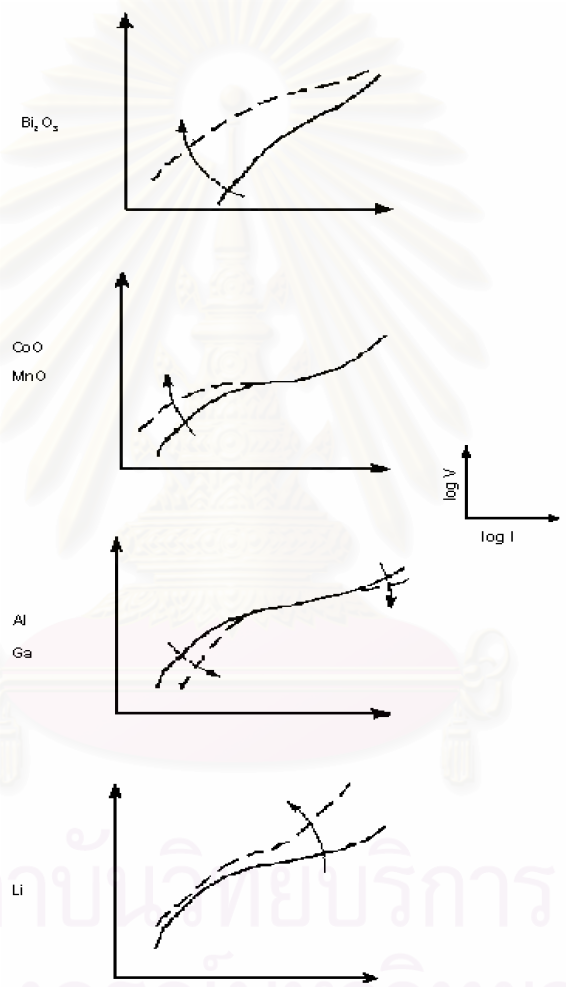

Figure 2.5 Effect of oxide additives on the shape of the current-voltage characteristic of ZnO varistor[4].

It should also be noted the leakage increases when the varistor is subjected to a hydrostatic pressure[14] or when the current frequently flows through it[15].

2.2.2 Physics of Zinc Oxide Varistors

The conduction mechanism of the ZnO varistors has been proposed to a large variety of models. Those models make neither a statement regarding the structure of the grain boundary nor a prediction of the effect of a change in composition or processing on the electrical behavior of the varistor. Therefore, the band models have not been very helpful in predicting the ways of improving the varistor properties. The electrical property of ZnO varistor has been developed by empiricism.

The progress of the conduction mechanism in a varistor[16] is summarized in Table 2.1. From these studies, the nonlinearity is recognized as a grain-boundary phenomenon where a barrier to the majority charge carriers, which are electrons, exists in the depletion layers of the adjacent grains. The most likely barrier at the grain boundary of the ZnO microstructure is the Schottky barrier[17] as shown in Figure 2.6.

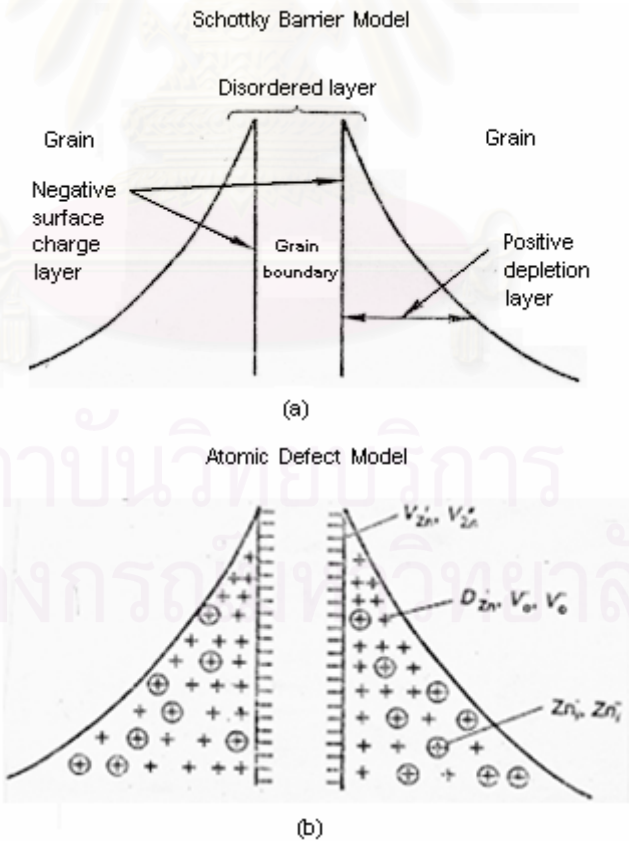

Figure 2.6 Grain-boundary atomic defect model analogous to Schottky Barrier model: (a) Schottky model and (b) atomic defect model[17].

Table 2.1 Progress in research in the conduction mechanism of ZnO Varistors[16].

Year	Model
1971	Space-charge-limited current (Matsuoka)
1975	Tunneling through a thin layer (Levinson and Philipp)
	Tunneling through Schottky barriers (Levine)
1976	Tunneling through Schottky barriers (Morris, Bernascone, et al.)
1977	Tunneling through Schottky barriers with heterojunctions (Emtage)
1978	Tunneling through Schottky barriers with heterojunctions (Eda)
	Tunneling through homojunctions (Einzinger)
1979	Tunneling through Schottky barriers (Hower and Gupta)
	Holes-assisted tunneling through Schottky barriers (Mahan, Levinson, and Philipp)
1982	Bypass effect at heterojunctions (Eda)
1984	Hole-induced breakdown (Pike)
1986	Bypass effect at heterojunctions (Levinson and Philipp)
	Hole-induced breakdown (Blatter and Greuter)
1987	Space-charge-induced current (Suzuoki et al.)

The basis for varistor characteristics is that electron transport across charged grain boundaries is dependent on voltage. The theory usually proposed describes the transport of majority carriers, which are electrons in the case of ZnO, across a charged grain boundary.

The current-voltage characteristics are controlled by the existence of an electrostatic barrier at the grain boundaries. According to Pike's paper[18], a grain boundary is referred to be formed by joining two identical semiconducting grains

together with an intervening layer of grain boundary material (Figure 2.7). The grain-boundary material is assumed to consist of the same semiconducting material with defects and dopants. As a result, its Fermi energy level differs from that of the two separated grains. And it also has eletronic states because of the defects and dopants within the band gap energy. In order to achieve thermodynamic equilibrium, electrons flow until the Gibbs free energy of an electron is equally everywhere. As illustrated in Figure 2.7, to increase the local Fermi level, electrons flow to the grain boundary and then are trapped by the defects and dopants until the Fermi level is the same throughout the material. At equilibrium, the chemical energy gained by an electron occupying a trap state is equal to the electrostatic energy spent in moving an electron from the grain interior to the boundary. Consequently, the trapped electrons act as sheet of negative charge at the boundary, leaving a layer of positively charged donor sites on either side of the boundary, and create an electrostatic field with a barrier at the boundary. The magnitude of the potential barrier can be calculated by solving the Poisson equation for the potential, $\Phi(x)$, from the knowledge of the grain-boundary charge density, $\rho(x)$:

$$\frac{d^2}{dx^2}\Phi(x) = \frac{\rho(x)}{\varepsilon\varepsilon_0} \tag{2.3}$$

where ε is the relative permittivity and ε_0 is the permittivity of free space.

The charge at a boundary can be represented by a sheet of trapped charge of local density (n_t). From the solution of the Poisson equation, the barrier height (Φ_B) and the width (d) of the depletion layer are given by the relations:

$$\Phi_B(V=0) = \frac{e^2 n_t^2}{8\varepsilon\varepsilon_0 n_0} = \frac{Q_i^2}{8e\varepsilon\varepsilon_0 n_0} \tag{2.4}$$

$$d = \frac{Q_i}{2n_0} \approx \left(\frac{\varepsilon\Phi_B}{n_0}\right)^{1/2} \tag{2.5}$$

where n_0 is the carrier concentration in the grains. When the voltage (V) is applied across the grain boundary, the band structure changes as expressed in Figure 2.8[1].

The current flows across the boundary are generally consistent with a thermionic emission process. Coincidentally, additional electrons can be trapped at the boundary, and there is a dynamic flow of trapped charges between the grains and the boundaries. The current density (J) is related to the applied voltage by the relationship:

$$J = A^{*}T^{2}\exp[-(e\Phi_{B}(V) + \varepsilon_{\xi})/kT]\exp(-eV/kT) \qquad (2.6)$$

where A* is the Richardson constant, T is the temperature, ε_{ξ} is the Fermi level in the adjoining grain, and k is the Boltzmann constant. The barrier height depends on the applied voltage and the energy distribution of interface states. Yet, it can be approximated in terms of a critical voltage, V_C, as followed.

$$\Phi_{B}(V) = \frac{V_C}{4}\left(1 - \frac{V}{V_C}\right)^{1/2} \qquad (2.7)$$

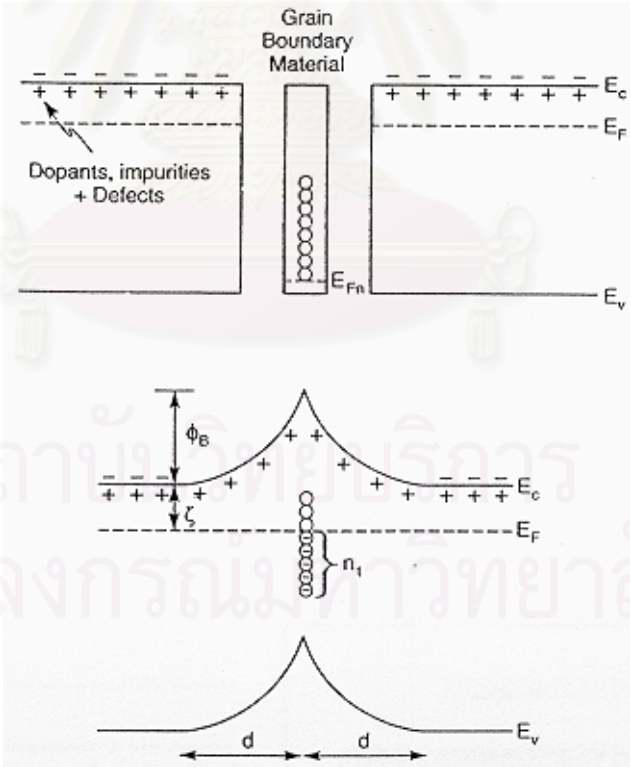

Figure 2.7 Formation of a potential barrier at a grain boundary[18].

As indicated by the equation (2.4) the barrier height decreases with increasing grain conductivity; accordingly, if the conductivity is too low, the barrier does

not exist. As the formation of the barrier requires a Fermi level difference between the grains and the boundary, if the Fermi level is too low, the states in the gap cannot be filled. Moreover, since the grains and boundaries are in series, if the conductivity is too low, the overall conductivity of the device is insufficient to be useful.

However, spatial variations in the charge along grain boundaries and in ionized donor distribution in the depletion region cause spatial variations in the barrier height and in the current density flowing across the barrier.

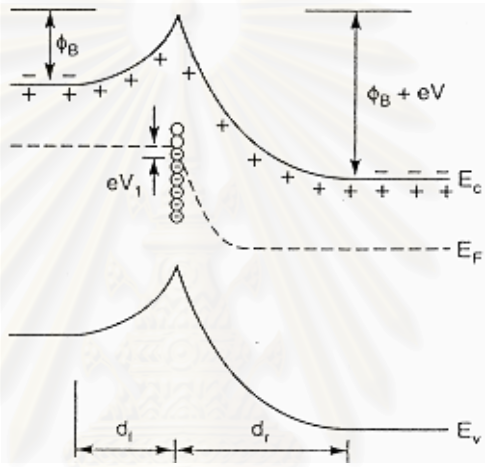

Figure 2.8 Schematic energy band structure at the grain boundary with applied voltage[1].

Since this explanation cannot realistically account for either the very large nonlinearity exhibited by varistor at small voltages per grain boundary. To describe this phenomenon, the generation of minority carriers by “hot” electrons in the depletion region at the high electric fields were also presented. This nonequilibrium process is shown in Figure 2.9[1]. Under very high electric fields, some electrons crossing the barrier gain sufficient kinetic energy so they can produce minority carriers by impact ionization of the valence states and acceptor states within the depletion region. The holes (minority carriers) diffuse back to the grain boundary under the influence of the electrostatic field at the grain boundary and compensate part of the trapped negative charge. Therefore, the potential barrier is lowered. The electron flow across the barrier increases. This impact ionization “feedback” process provides a high

degree of nonlinearity in the electron transport across the grain boundary and brings about very large nonlinear coefficients.

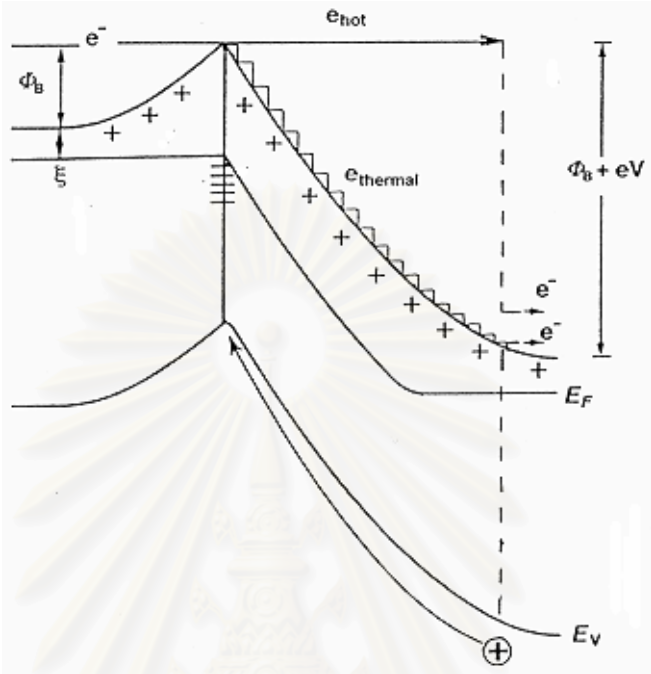

Figure 2.9 Energy band diagram for a grain boundary under applied voltage, illustrating the interband impact ionization process and the hole generation. Holes are drawn to the grain boundary to compensate the trapped negative charge and lower the potential barrier[1].

There is a limitation of the double Schottky barrier model. It attempts only to describe electron transport across an individual grain boundary; however, varistors are polycrystalline materials containing a large number of individual boundaries, each of which has different characteristics.

2.2.3 Chemistry of Zinc Oxide Varistors

The crystal structure of ZnO is shown in Figure 2.10[17]. Zinc oxide crystallizes in the hexagonal lattice of wurtzite in which the oxygen atoms are arranged in a hexagonal close-packed type with zinc atoms occupying half the tetrahedral sites. The zinc and oxygen atoms are tetrahedrally coordinated to each other and are, therefore, equivalent in position. The structure is thus relatively open with all the octahedral and half of the tetrahedral sites are empty. Therefore, it is easy to

incorporate external dopants into the ZnO lattice as is observed in a varistor. The open structure involves the nature of defects and the mechanism of diffusion. The most common defect in ZnO is the metal interstitial leading to a nonstoichiometric metal excess n-type semiconductor. Figure 2.11[17] represents the band structure of ZnO. The band gap of ZnO has been determined to be 3.3 eV and thermodynamically formed natural defects occupy the donor and acceptor levels within the band gap. The interstitial (Zn_i) has the fastest diffusion rate among the natural defects and plays an important role in varistor stability.

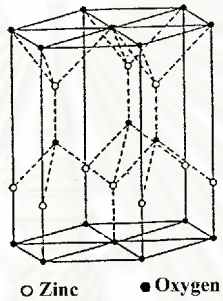

Figure 2.10 ZnO crystal structure[17].

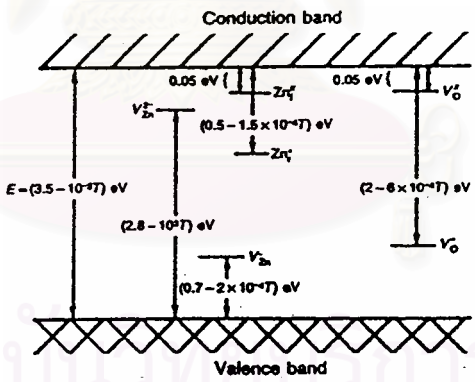

Figure 2.11 Electronic energy levels of native imperfection[17].

In ZnO varistor, the atomic defects are formed by oxide additives incorporating at the grain and the grain boundary. The donor or donor-like defects dominate the depletion layer while the acceptor or acceptor-like defects dominate the grain boundary state. The relevant defect species are the zinc vacancies (V_{Zn}' and V_{Zn}''), the oxygen vacancies ($V_{\dot{O}}$ and $V_{\ddot{O}}$), the zinc interstitial atoms (Zn_i and $Zn_{\ddot{i}}$), and the externally incorporated donor and acceptor atoms ($D_{Zn}^{\cdot}$ and D_i').

Einzinger[19] has demonstrated that a defect-induced potential barrier can be formed from the unequal migration of defects toward the grain boundary, without the requirement of a physically separating intergranular layer to account for the barrier as pointed out by Matsuoka[7]. It was found that, with a substantial donor doping ($D_{Zn} \approx 10^{18}$ cm^{-3}), the grain boundary became rich in zinc vacancy concentration $[V_{Zn}]$ and poor in oxygen vacancy concentration $[V_O]$ during cooling from high sintering temperature. This doping brought about an excess of $[V_{Zn}]$ and a deficit of $[V_O]$ at the grain boundary. This condition gave rise to a barrier at the depletion layer, so a separate interface layer at the grain boundary was not required.

The chemistry of the ZnO varistors can be summarized as follows[17].

1. There is a charge separation at the grain boundary of the ZnO varistor as a result of cooling from the sintering temperature.

2. The native donor concentrations: $[Zn_i^{\cdot}]$ and $[Zn_i^{\cdot\cdot}]$, $[V_O^{\cdot}]$ and $[V_O^{\cdot\cdot}]$, are depressed while the acceptor concentrations; $[V_{Zn}^{\prime}]$ and $[V_{Zn}^{\prime\prime}]$, are enhanced.

3. In the grain boundary region, the deep donors, $D_{Zn}^{\cdot}$, were found and the mobile electrons were nearby markedly depleted.

2.2.4 Microstructure of Zinc Oxide Varistors

The ZnO varistors usually contain the bismuth oxide (Bi_2O_3) as a varistor and other metal oxides such as Sb_2O_3, Co_2O_3, SiO_2,the additional dopants. Bi_2O_3, which has low melting temperature of 825°C, causes the liquid-phase sintering. As a result, the microstructure of varistors consists of large ZnO grains with a bismuth-rich second phase at the grain boundaries. In addition, a bismuth-rich phase is found as the insulating three-dimensional network, as shown in Figure 2.12[1].

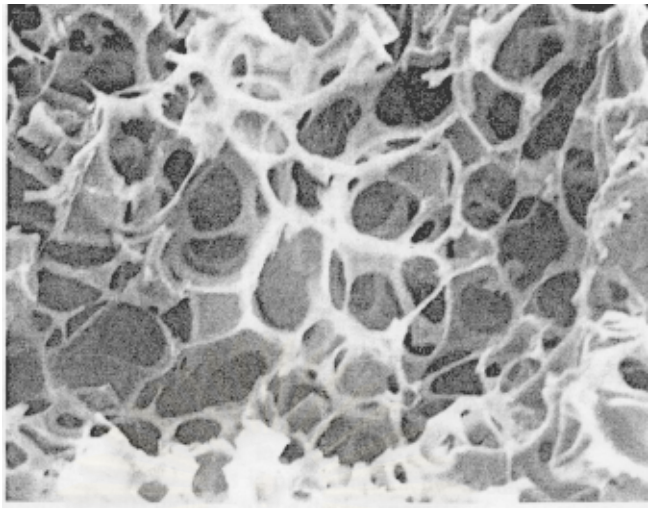

Figure 2.12 Three dimensional insulating intergranular layer of ZnO varistor after leaching ZnO grains with acid[1].

From the details above, the conducting ZnO grains separated by the insulating grain boundaries are firstly predicted as presented in Figure 2.13[31]. However, the complexity of the composition results in the more complex microstructure than that from theoretical model. Figure 2.14[20] shows a photomicrograph of the polished and etched section of the commercial varistor. Its microstructure contains ZnO grains, accompanied by twins delineating different ZnO crystal planes, the intergranular phase, particles and pores. The comparison of second phase varies with the overall chemical formulation, processing times and temperatures. This suggests that they are repositories for excess dopants not taken into solution within the ZnO grains or segregated to the grain boundaries. However, the bismuth-rich phase appears to have particular importance, since there are reports suggesting the varistor characteristics are related to the particular crystalline formed Bi_2O_3 phase[21,22]. Although the phase transformations in pure Bi_2O_3 are presented in Figure 2.15[23], the Bi_2O_3 phases forming from the liquid phase sintering contain several dissolved elements, such as antimony, zinc, and cobalt.

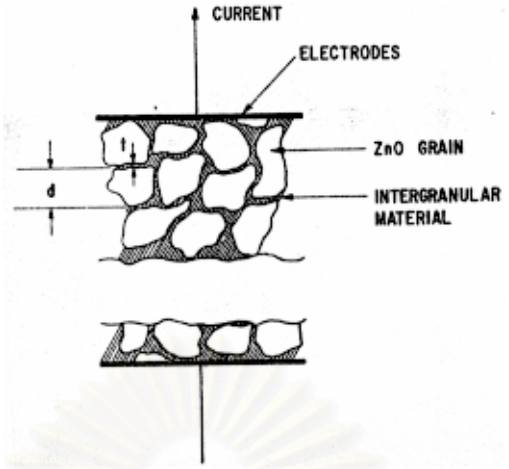

Figure 2.13 Schematic illustration of the microstructure of a ZnO varistor[20].

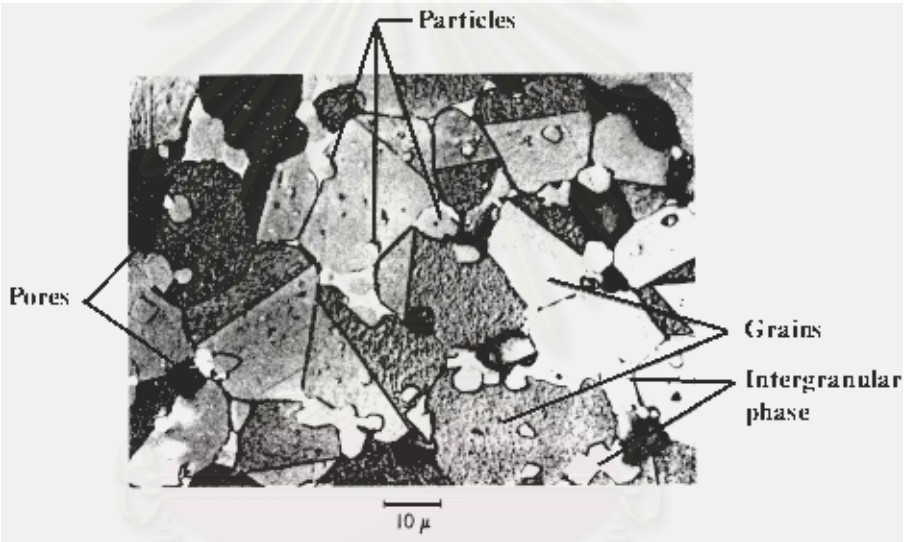

Figure 2.14 Optical photomicrograph of a polished and etched section of a commercial varistor[20].

Four stages can be distinguished associated with the fabrication of varistor. First, a liquid phase forms during heating of the powder. The second phases such as pyroclore and spinel can also form, depending on time, temperature and formulation at this stage. The dissolution and diffusion of dopants continue to provide a uniform dopant distribution. Second, liquid-phase densification and grain growth occur. To obtain the composition uniformity including densification and grain size, the appropriate sintering temperatures and times should be specified. Third, during cooling to the intermediate temperature, crystallization of the secondary phases from the

bismuth-rich liquid phase and the retraction of the liquid phase from the two grains bonds to the triple junction occur. Finally, further cooling (from 700°C to 450°C) with slow rate or subsequent annealing in this temperature range leads to the development of the electrical properties. This heat treatment is a key feature of the fabrication of varistor, especially for high voltage applications. The annealing stage is necessary for both the attainments of a high nonlinearity and stability against degradation[1].

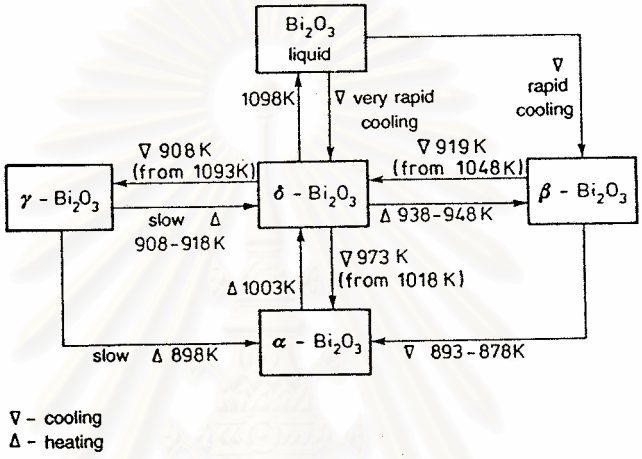

Figure 2.15 Schematic diagram illustrating the phase transformation in pure Bi_2O_3[23].

2.3 Fabrication of Zinc Oxide Varistors

The Bi-doped ZnO varistors are usually prepared by liquid phase sintering ZnO powder with Bi_2O_3 and other additives such as antimony, manganese, cobalt, silicon and aluminium oxides. The traditional ceramic techniques are normally used to produce the ZnO varistor[24,25] (Figure 2.16).

The fabrication process starts with weighing the stoichiometric amount of the oxide powder and mixing into the homogeneous mixture. Then, the mixed powder is pressed into the desired shape such as a disk and then fired at high temperature, typically; 1100-1400 °C. Finally, the fired or sintered pellets are electroded usually with a fired silver contact and attached with leads by soldering before finished with epoxy encapsulation. After fabrication, the finished product was tested.

In addition, the preparation of the ZnO varistor powder is alternated to obtain the high voltage varistors. The precursor powder is prepared by calcining the mixed powder at the temperature of 800-900°C. After that, the calcined powder is wet milled and dried before pressing.

Today, the preparation process of ZnO varistors is developed for many purposes such as to obtain the better homogeneity, to lower the sintering temperature, or to prepare the different shape.

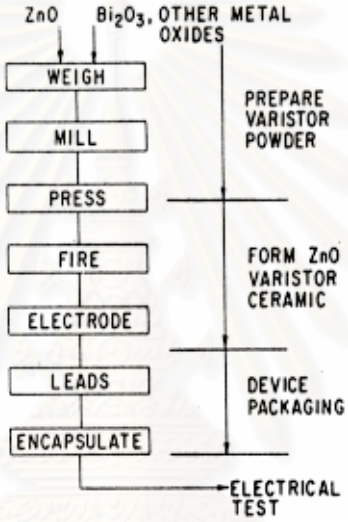

Figure 2.16 Simple fabrication diagram of ZnO varistors[24,25].

2.4 Applications of Zinc Oxide Varistors

The ZnO varistors used as the transients protective devices are directly connected across the power line in parallel with the load to be protected as shown in Figure 2.17. In addition to their highly nonlinear behavior, a significant advantage of them derives from the ceramic nature of the material. Because of their polycrystalline with energy absorption occurring essentially at the grain boundaries distributed throughout the volume of the material, ZnO varistors are inherently able to absorb more energy than single-junction protective devices such as Zener diodes. The capability to absorb thosed energy is in hundreds of J/cm^3.

A second good feature is an ability to configure a particular device to conform to system constraints. A various size and shape of the ZnO varistors can be formed. For example, a miniature sleeve fabricated as a tube that can be fit around a connector pin, a miniature chip varistor and the large volume of varistor used in power system protection can be made.

The requirements of the varistor for their applications are:

1. high nonlinear coefficient,
2. suitable breakdown voltage,
3. low leakage current,
4. long life or high stability, and
5. high energy absorption capability.

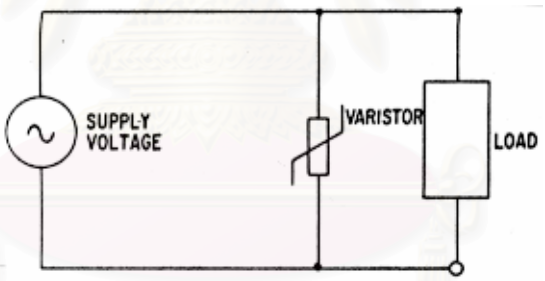

Figure 2.17 Typical application of ZnO varistor as a transient protective element.[24,25]

CHAPTER 3
EXPERIMENTAL PROCEDURE

Varistor materials used in this study were ZnO ceramic varistors. The 95 wt% ZnO - 5 wt %Bi_2O_3 system was chosen as the base composition. The nonlinear coefficient (α) reported by Asokan and coworkers in 1987 was 13.4[26]. The suitable sintering condition of this composition with less than 5 %Bi_2O_3 concentration was 900 °C with a soaking period of 2 hours in the ambient air to obtain the optimum properties. This condition was employed in this study. The different atmosphere was also applied during sintering.

BaO was selected as a dopant in this composition. It was found to enhance the grain size, resulting in an increase of the nonlinear coefficient. Fan and Freer (1997)[27] confirmed that the result of BaO increased the nonlinear behavior of ZnO ceramics. The highest α of 0.78 mol% BaO doped composition sintered at 1300 °C for 1 hour was 14.

Consequently, the effects of BaO addition up to 1 wt% on the properties of 95%ZnO-5%Bi_2O_3 were studied.

3.1 Material Preparation

The compositions investigated in this research were :

1) 95 % ZnO - 5 % Bi_2O_3 as the base composition,

2) 0.5 wt%BaO-doped base composition, and

3) 1.0 wt%BaO-doped base composition.

The samples were synthesized by following method (Figure 3.1).

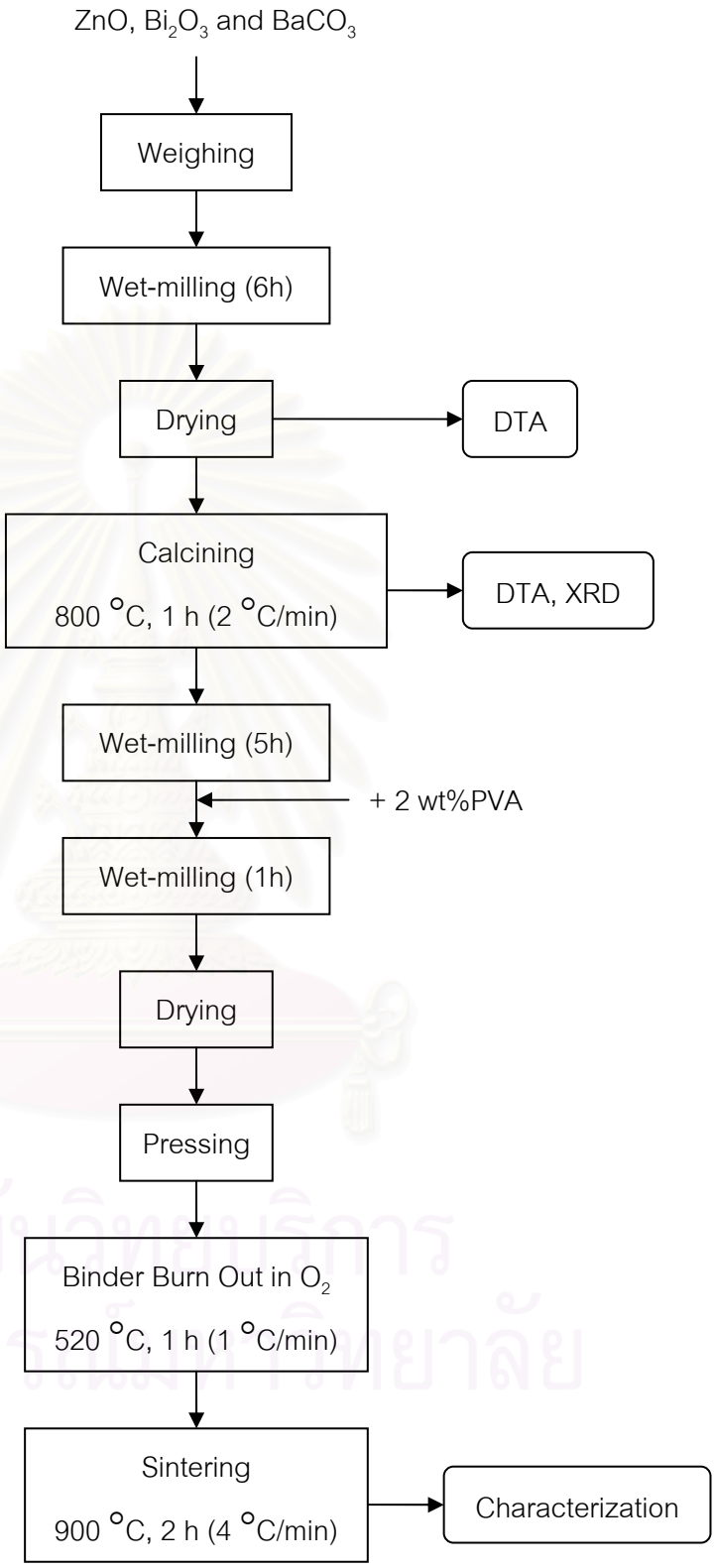

Figure 3.1 Flow chart of the experimental procedure.

(1) The reagent grade ZnO (RIEDEL-DE HAEN), Bi_2O_3 (RIEDEL-DE HAEN) and $BaCO_3$ (BAKER ANALYZED) were weighed in the proportion amounts providing the designed compositions.

(2) All starting materials were mixed and milled for 6 hours in a high density polyethylene bottle with zirconia balls as a grinding media and ethyl alcohol as a solvent.

(3) The mixture was dried and then calcined in air. The calcining schedule was determined by the differential thermal analysis (DTA).

(4) The calcined powder was ball milled for 6 hours and 2 wt% polyvinyl alcohol (PVA) acted as binder were added in the last milling hour.

(5) The dried powder was pressed into disks by cold isostatic pressing (CIP).

(6) The binder was burned out at 520°C for an hour with a heating rate of 1 °C/min in oxygen.

(7) All samples were sintered at 900 °C for 2 hours with a heating rate of 4 °C/min in air and oxygen.

3.2 Material Characterization

3.2.1 Thermal Analysis

To identify the suitable calcining temperature, the differential thermal analyzer (PERKIN ELMER DTA7) was used. The mixed oxide powder was placed in the sample crucible and alumina was used as the reference material. The data were taken from room temperature to 1200 °C with a heating rate of 10 °C/min.

After calcining, the powder was rechecked for the complete reactions with the same procedure. If there is no peak existed, the reactions are complete.

3.2.2 Phase Determination

The phases of the calcined and sintered samples were determined by X-ray diffraction. The calcined powder or sintered pellet was placed in the X-ray diffractometer (JEOL JDX 3530) and the data were collected from 20 to 90 degree of two theta with step angle of 0.02 degree and a counting time of 0.5 sec. The data obtained were matched with the JCPDS data files and finally the phases were identified.

3.2.3 Bulk Density Determination

The Archimedes method was used to determine the bulk density of the sintered disks. The bulk density (B) was calculated from the equations followed:

$$B, g/cm^3 = D/V \tag{3.1}$$

$$V, cm^3 = \frac{(W - S)}{\text{density of liquid}} \tag{3.2}$$

where D = dry weight (g)

V = exterior volume (cm^3) calculated from the equation (3.2),

W = saturated weight (g), and

S = suspended weight (g).

3.2.4 Microstructure Characterization

The scanning electron microscope (JEOL JSM-5410LV) was used to study the microstructure of the sintered sample. The sample was polished down to 1 micron and then thermally etched at 800 °C and 900 °C (for samples sintered at 900 °C and 1000 °C, respectively) for 2 hours with a heating rate of 4 °C/min. Gold (Au) as an electrode was sputtered on its polished surface before investigation.

3.2.5 Current-Voltage (I-V) Measurement

The I-V relation was obtained by collecting the currents at the several applied voltages. The power supply and the microampmeter used in this measurement were set up as illustrated in Figure 3.2. The data were converted into the current densities (A/cm^2) and the applied fields (V/cm) by dividing the current with an area of electrode and the voltage with a distance of electrode separation. The data curve on a logarithmic scale was used to determine the nonlinear coefficient (α). The bulk resistivity was estimated from the slope in the prebreakdown region in linear scale. The α-value was calculated from the reciprocal of the slope in the nonlinear regime as shown in the equation (3.3).

$$\alpha = \frac{\log (I_2 / I_1)}{\log (V_2 / V_1)} \tag{3.3}$$

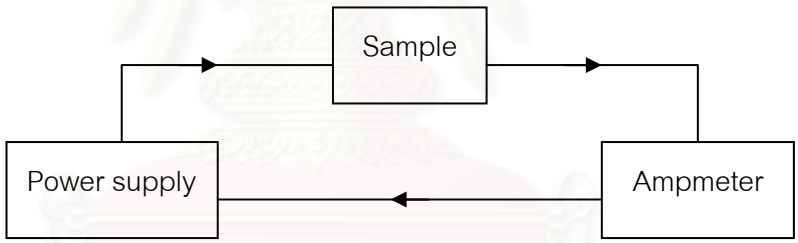

Figure 3.2 Diagram of the current-voltage (I-V) measurement; the arrow represents the direction of the current flow.

CHAPTER 4
RESULTS AND DISCUSSION

4.1 Thermal Analysis

To determine the appropriate calcining schedule of 95%ZnO-5%Bi_2O_3 base composition, the reaction peaks of the stoichiometric mixture of ZnO, Bi_2O_3 and $BaCO_3$ were detected by DTA. The thermal analysis results of undoped and Ba-doped base composition were shown in Figure 4.1. As indicated by the two exothermic peaks, the reactions occurred around 315 °C and 800 °C for undoped sample. However, with 1 wt% of BaO additive, the second reaction peak shifted to a lower temperature. This may indicate that Ba was attributed to the reaction of this solid solution at high temperature. The observed peak at lower temperature was associated with the reaction of Bi_2O_3 as expected for all compositions with this additive oxide. According to this result, the proposed calcining schedule was to increase the temperature to the presence of the reaction peaks and soaking at each reaction temperature was still necessary for a large amount of powder to complete the reaction. Nevertheless, the actual first soaking temperature was 300 °C instead of 315 °C since a slow heating rate of 2 °C/min, not 10 °C/min as used in DTA, was set in the program controller. In general, a slow heating rate shifts the reaction peaks toward lower temperature.

Figures 4.2, 4.3 and 4.4 show the results of DTA traces for calcined powder of undoped and Ba-doped compositions. Although two small humps as obviously shown on the derivative curve of Figure 4.3 could be observed at the same reaction temperatures of calcined powder, they were not significant since after forming it was sintered to 900 °C with two hours soaking at this temperature.

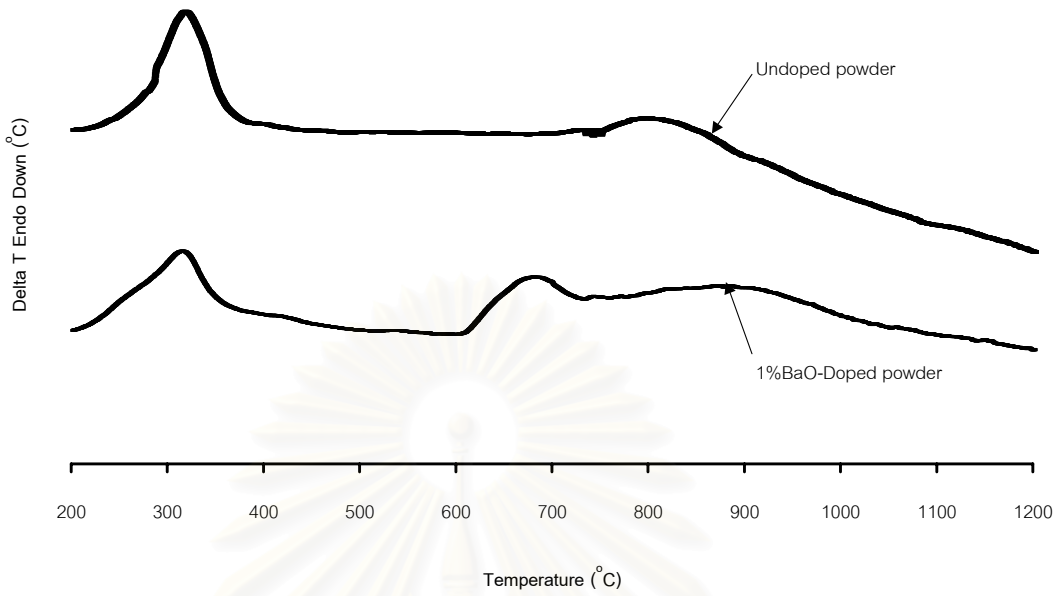

Figure 4.1 DTA curves of mixed powders of undoped and 1% BaO-doped base compositions.

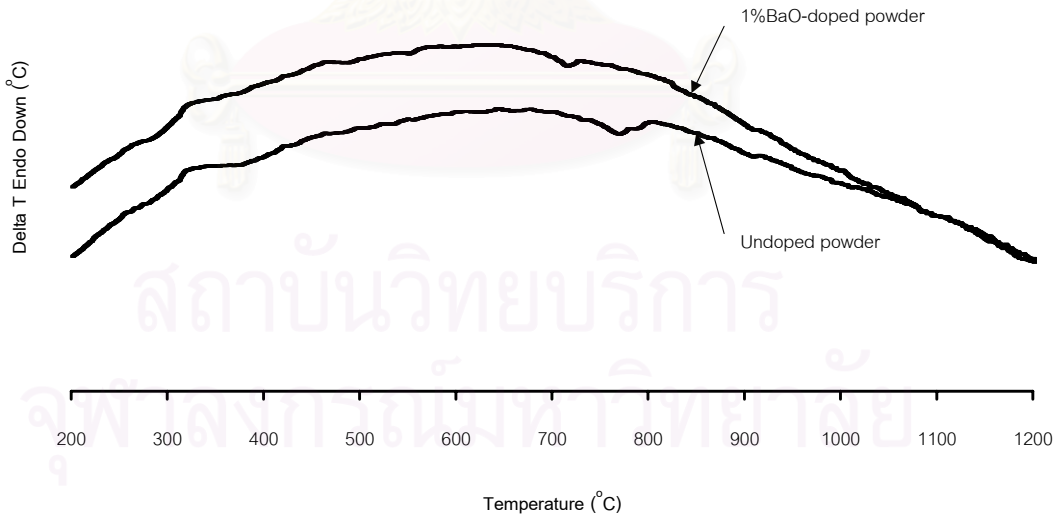

Figure 4.2 DTA curves of calcined powders of undoped and 1 %BaO-doped-base compositions.

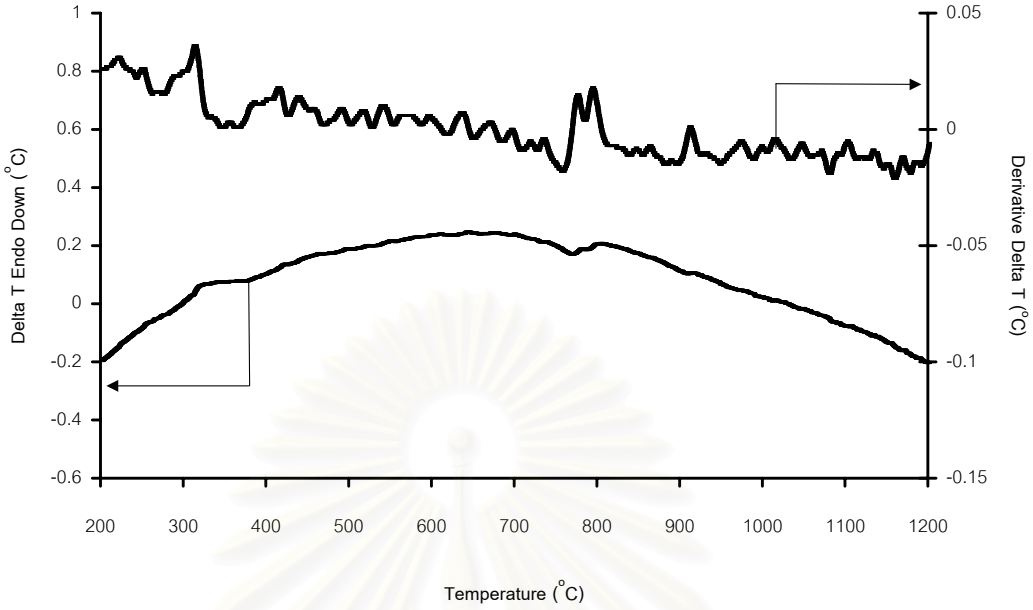

(I) For undoped base composition

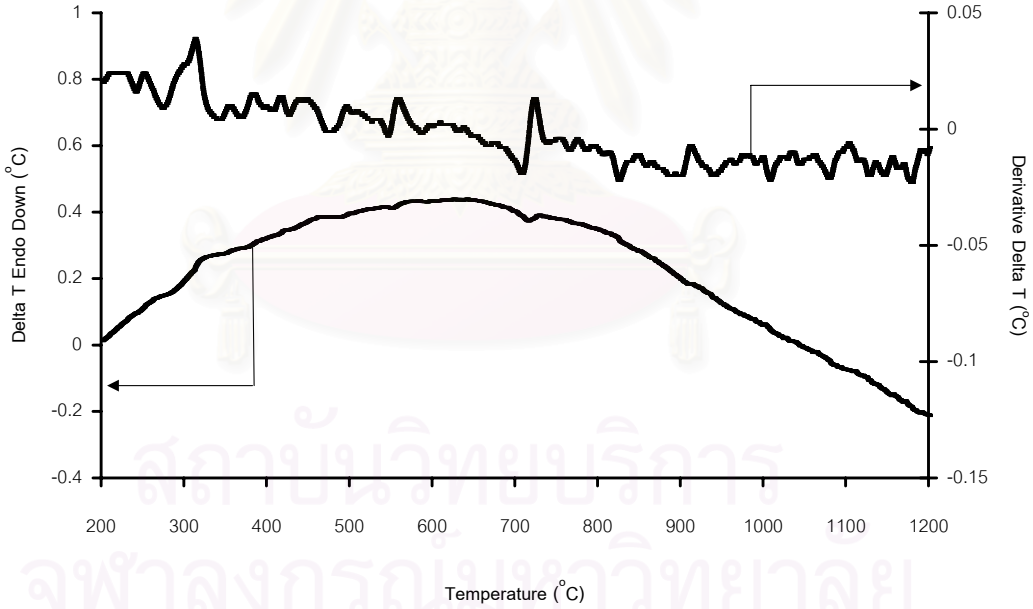

(II) For 1 %BaO-doped based composition

Figure 4.3 DTA curves and derivative curves of calcined powders of undoped and 1 %BaO-doped 95%ZnO-5%Bi_2O_3 base compositions.

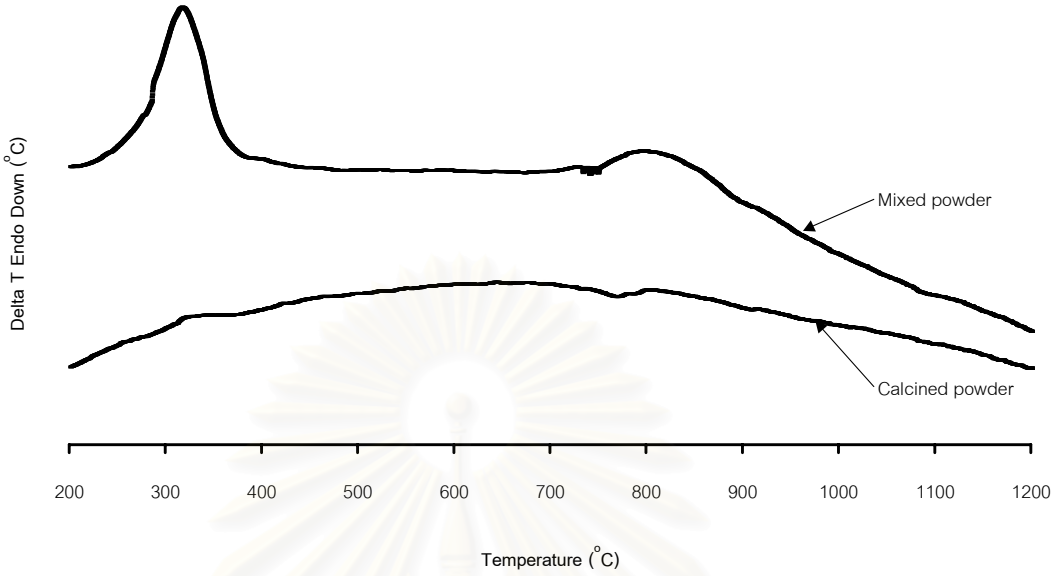

(I) For undoped base composition

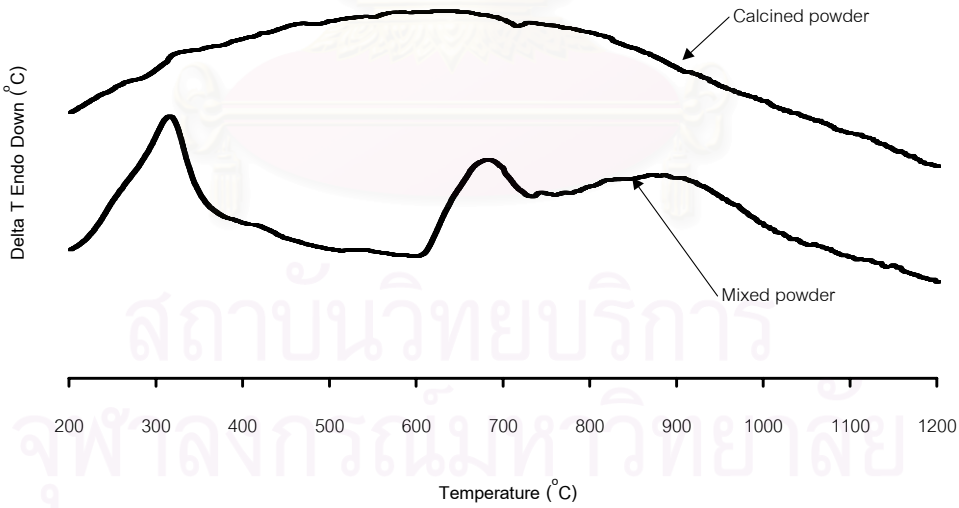

(II) For 1 %BaO-doped based composition

Figure 4.4 DTA curves of mixed and calcined powders of undoped and 1 %BaO-doped 95%ZnO-5%Bi_2O_3 base compositions.

4.2 Effect of Barium Oxide Dopant and Sintering Atmosphere

4.2.1 Crystal Phases

The results of XRD patterns for both of calcined powder and sintered pellet are shown on Figures 4.5 and 4.6, respectively. The major and minor phases for calcined powder of undoped and doped with 1 wt% of BaO are similar. They were identified to be the hexagonal ZnO as appeared in JCPDS no. 36-1451 (Appendix A) and the bismuth-rich phases. These phases are possible either various polymorphs of bismuth oxide phases or zinc bismuth oxide phases since the existing peaks for both are almost exactly at the same two-theta (Appendix B). This result is in good agreement with previous works[28-34]. After sintering at 900 °C for two hours, the phases presented in the sintered sample are still unchanged as illustrated in Figure 4.7. The X-ray diffraction pattern of the samples sintered in oxygen also shows an unknown bismuth-rich phase at 30 ° two-theta. With an increasing amount of BaO, the intensity peak height at this two-theta increases. This may imply that Ba prevents the evaporation of Bi, which generally occurs at 800-850 °C. Similar effect can be observed in the samples sintered in air as shown in Figure 4.8. Based on these results, comparison between sintering in oxygen and air, the formation of phases is independent of sintering atmosphere.

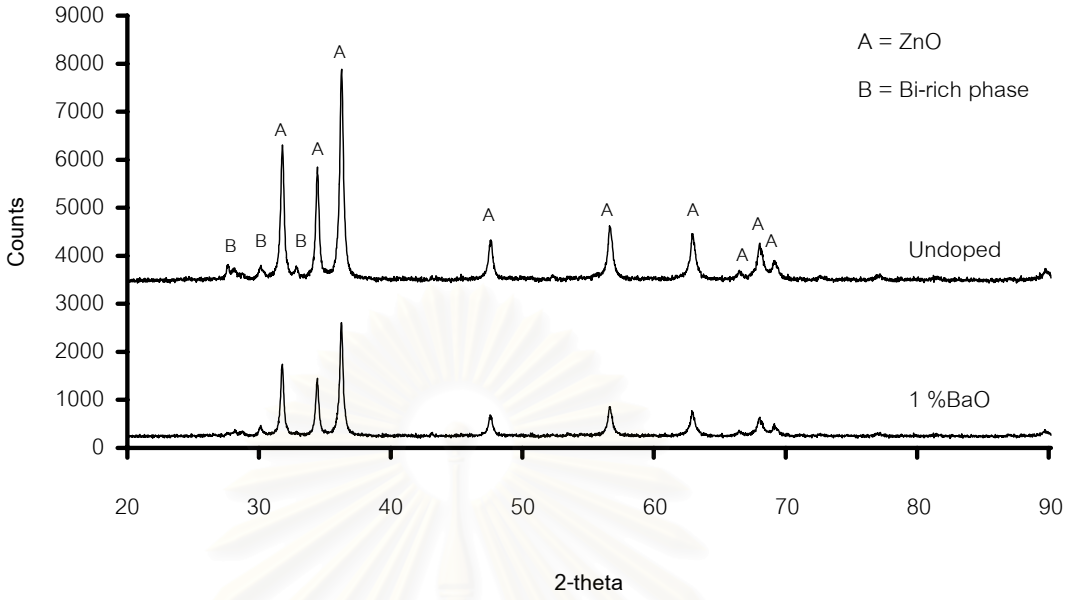

Figure 4.5 XRD patterns of calcined powders of undoped and 1 %BaO-doped base compositions.

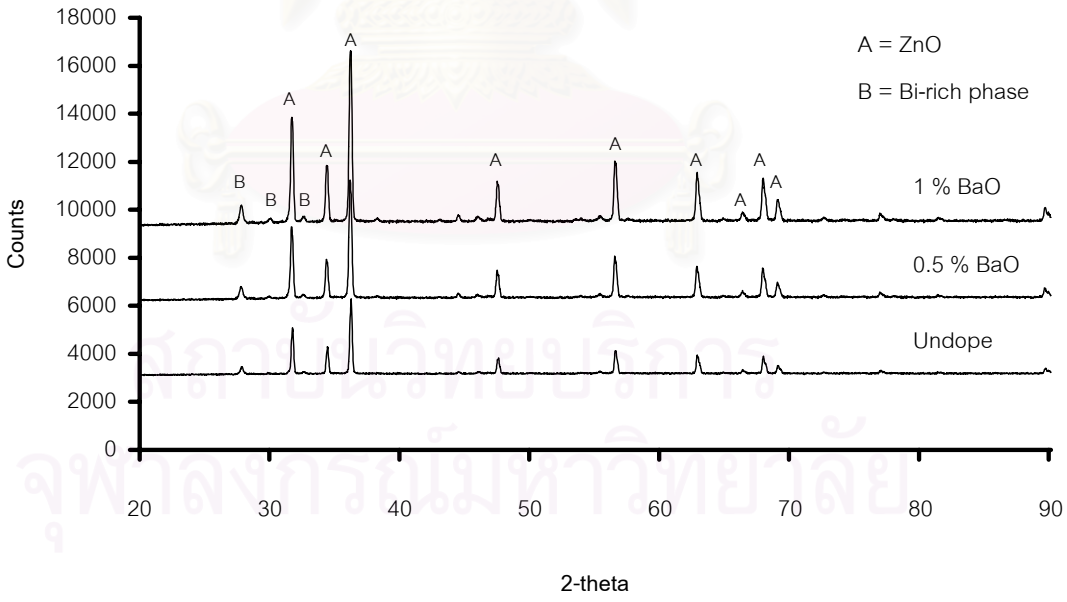

Figure 4.6 XRD patterns of pellets sintered at 900°C for 2 hours in oxygen.

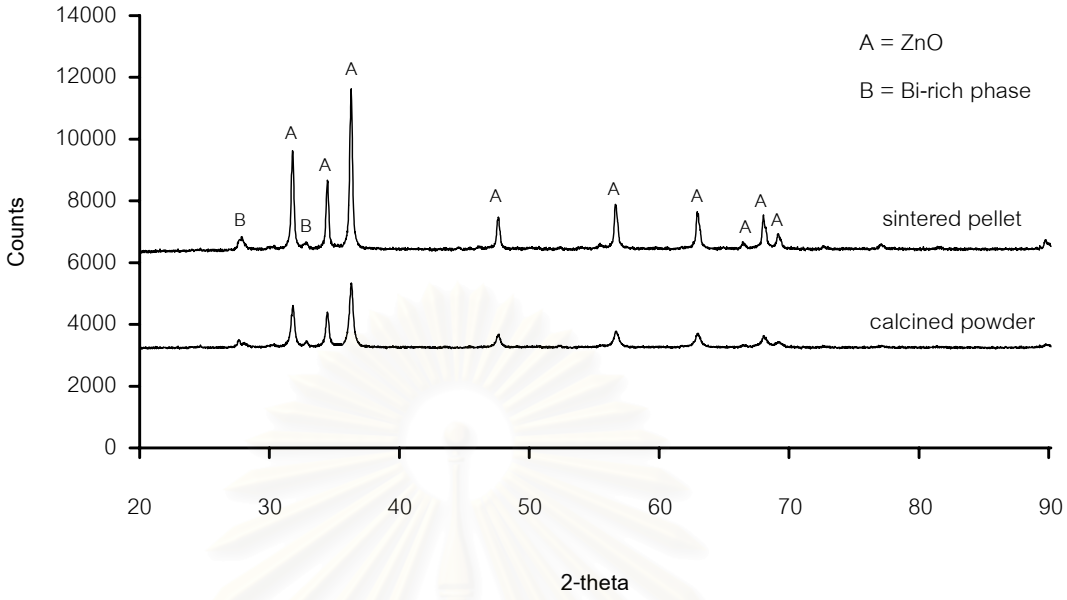

(I) For undoped base composition.

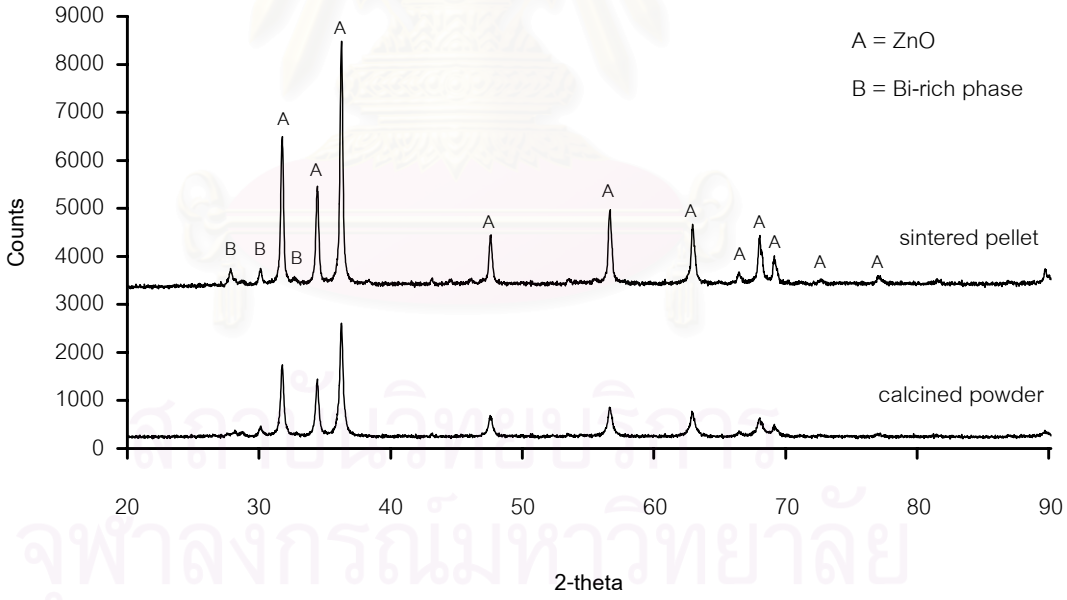

(II) For 1 %BaO-doped base composition.

Figure 4.7 XRD patterns of calcined and oxygen-sintered samples.

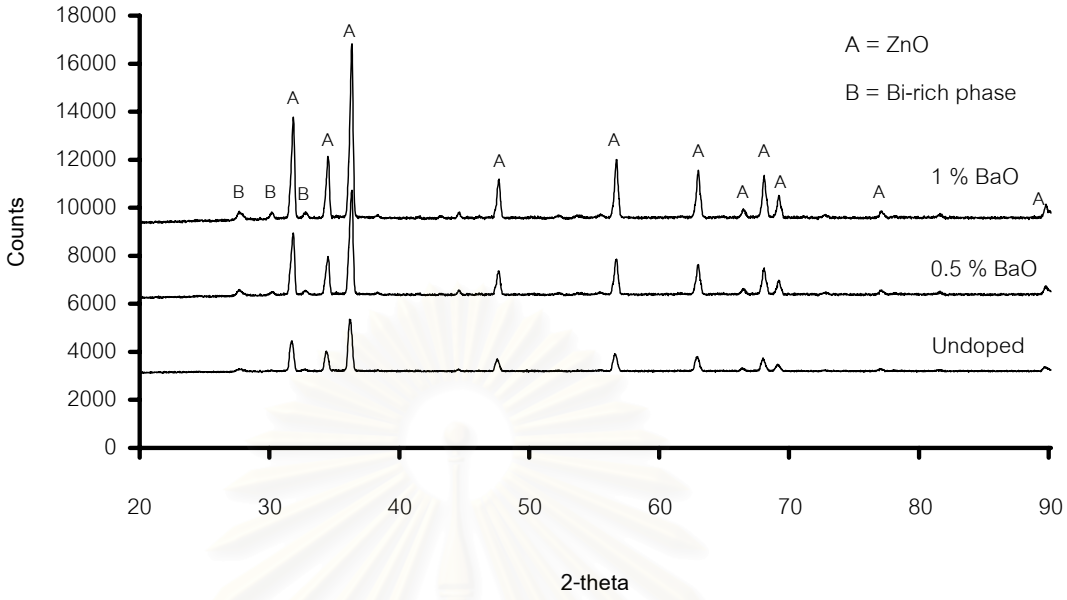

Figure 4.8 XRD patterns of pellets sintered at 900°C for 2 hours in air.

4.2.2 Bulk Density

The bulk density of the sample was determined by Achemides method and their results as a function of sintering atmosphere and %BaO are shown in Table 4.1. The sintering atmosphere obviously affects the density of samples. Higher density can be obtained if sintering in oxygen. Doped with BaO, the density of the samples decreases. This indicates that the higher sintering temperature is required for Ba-doped composition to achieve the optimum density.

Table 4.1 Bulk density of 95%ZnO-5%Bi_2O_3 ceramics doped with BaO up to 1 wt% sintered at 900 °C for 2 hours in air and oxygen.

% BaO	Bulk Density (g/cm^3)	
	Sintered in Air	Sintered in Oxygen
0	5.5	5.8
0.5	5.4	5.7
1	5.4	5.6

4.2.3 Microstructure

Figure 4.9 represents SEM photomicrographs of polished samples after sintering at 900 °C in oxygen. The microstructure of undoped base composition of 95%ZnO-5%Bi_2O_3 contains the second phase as appeared on the matrix grains and at the grain boundaries. As supported by the X-ray diffraction results, this should be any form of bismuth-rich phases. With 0.5 %BaO additive, the second phase apparently increased. This still persists in the sintered composition with 1 %BaO additive. Furthermore, the grain size tends to grow with an addition of BaO, thus enhancing the number of pores in the grains and at the grain boundaries. In other words, the formation of second phase associated with the larger grains may influence on the density.

Figure 4.10 shows SEM image of 0.5 %BaO-doped composition after sintering in air. It is clearly confirmed that the samples sintered in air have lower density than those in oxygen as compared to Figure 4.9 (II).

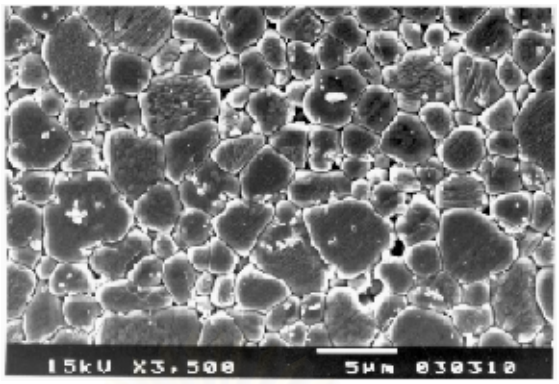

(I) For undoped base composition.

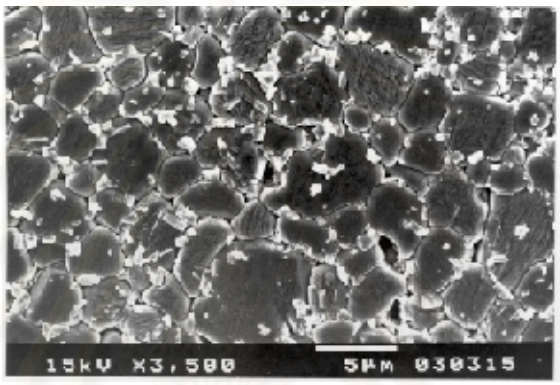

(II) For 0.5 %BaO-doped base composition.

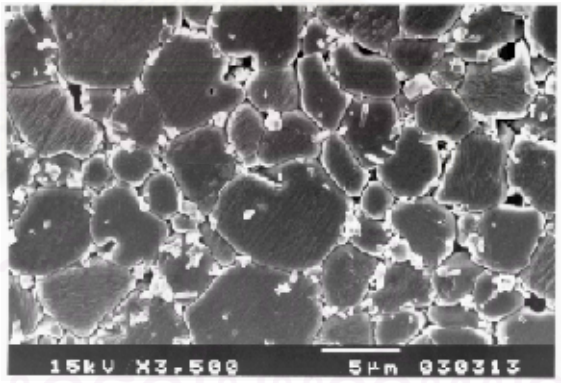

(III) For 1 %BaO-doped base composition.

Figure 4.9 SEM photomicrographs of polished samples sintered at 900°C for 2 hours in oxygen.

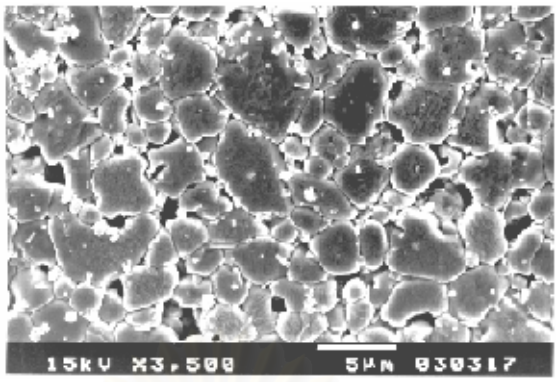

Figure 4.10 SEM photomicrograph of 0.5 %BaO-doped composition sintered in air at 900°C for 2 hours.

4.2.4 Current–Voltage (I-V) Characteristics

In order to evaluate the nonlinear electrical behavior varistor consisting of 5 wt% of Bi_2O_3 and from 0 to 1 wt% of BaO, the I-V curve was carried out. As far as the effect of sample dimension on electrical properties is concerned, the applied electric field versus current density is usually plotted for electrical characteristics of materials. The results of I-V curve for all undoped and Ba-doped compositions sintered at 900 °C in both oxygen and air are plotted in Figures 4.11 and 4.12, respectively. In the first region, the I-V characteristic displays the ohmic behavior for all compositions as shown in Figure 4.13. The current is proportional to the applied voltage in this prebreakdown region. The slope of this straight line can be used to determine the bulk resistivity of the sample. The bulk resistivity, which is the sum of resistivities obtained from ZnO grains, grain boundaries, second phases including pore, as a function of %BaO additives and sintering atmosphere is also given in Table 4.2.

The results show that the resistivity of composition sintered in oxygen increases as %BaO additive increases. In contrast to those sintered in air, the resistivity decreases as % BaO increases. This may be because bismuth acted as an insulating barrier cannot evaporate from the compositions doped with BaO and sintered in oxygen. Hence, the resistivity should increase with the amount of BaO. However, pores occur in the samples sintered in air resulting in decrease of resistivity. In addition, either

vacancies of oxygen or zinc interstitial atoms may introduce electrons in the low partial pressure of oxygen, corresponding to increase the conductivity.

Table 4.2 Bulk resistivity as a function of %BaO additive and sintering atmosphere of 95%ZnO-5%Bi_2O_3 sintered at 900 °C for 2 hours.

% BaO	Bulk Resistivity (Ω.cm)	
	Sintered in Air	Sintered in Oxygen
0	6.0×10^9	0.7×10^9
0.5	3.0×10^9	2.0×10^9
1	0.7×10^9	5.0×10^9

Table 4.3 Nonlinear coefficient as a function of %BaO additive and sintering atmosphere of 95%ZnO-5%Bi_2O_3 sintered at 900 °C for 2 hours.

% BaO	Nonlinear Coefficient (α)	
	Sintered in Air	Sintered in Oxygen
0	2.7	4.8
0.5	4.1	4.8
1	4.2	5.4

In the breakdown region or nonohmic behavior, the empirical power law is used to determine the nonlinear coefficient (α). The coefficient values for all compositions are also presented in Table 4.3. The maximum α of about 5 is found in the composition doped with 1 %BaO sintered in oxygen atmosphere. With air sintering,

BaO addition increases the nonlinear coefficient (α). This observation is consistent with the previous study[27]. Likely, the samples sintered in oxygen also have higher α with higher BaO content. These might be due to the increasing in grain size. Since the larger grain size might increase the conducting region in the bulk sample, after breakdown, the high current passed through these large conducting grains.

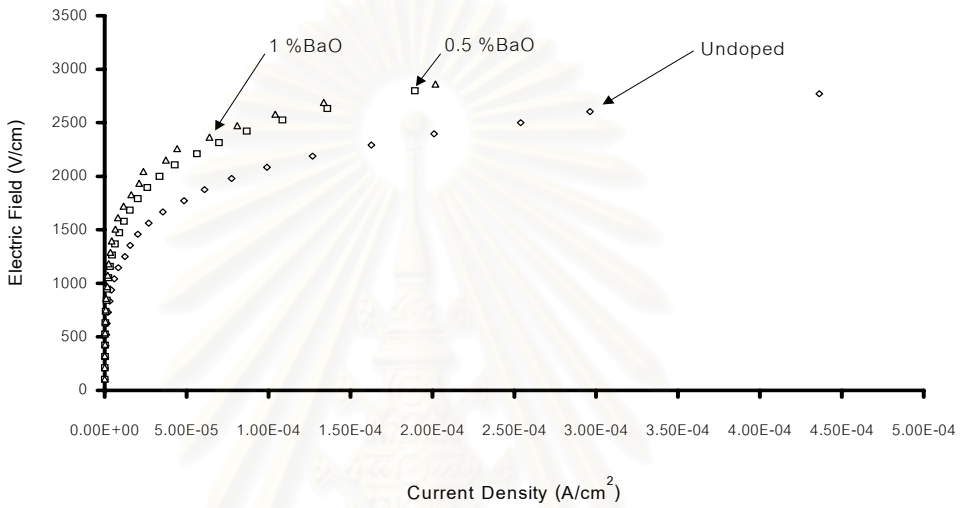

(I)

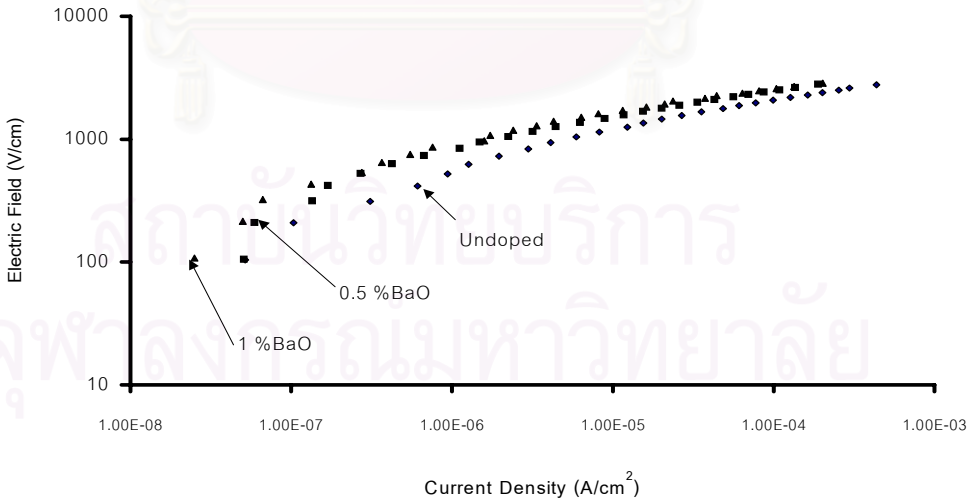

(II)

Figure 4.11 Current-voltage characteristics of doped and BaO-doped compositions sintered at 900°C for 2 hours in oxygen (I : Linear scale ; II : Logarithmic scale).

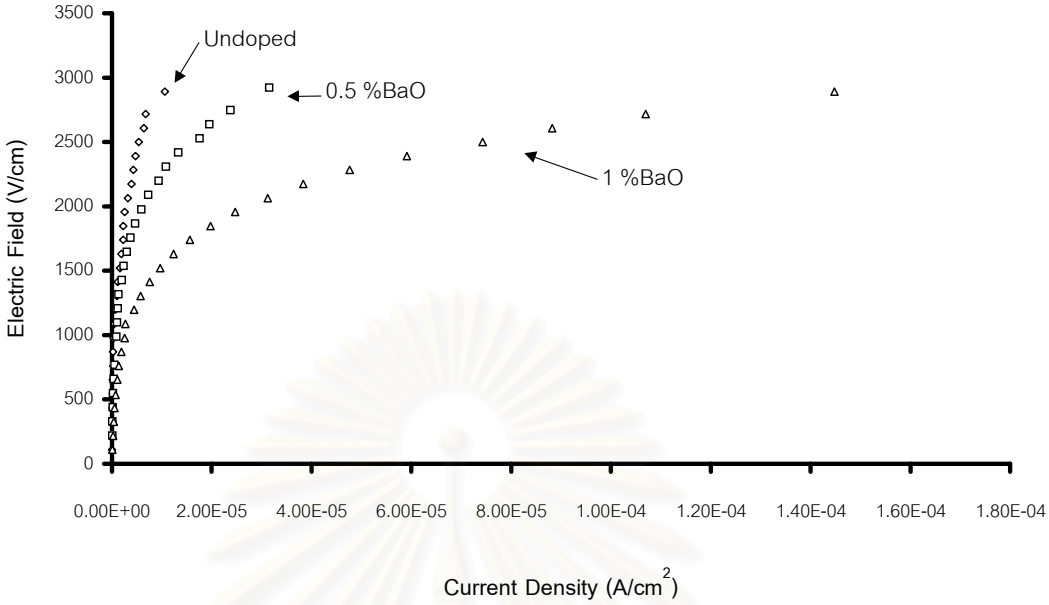

(I)

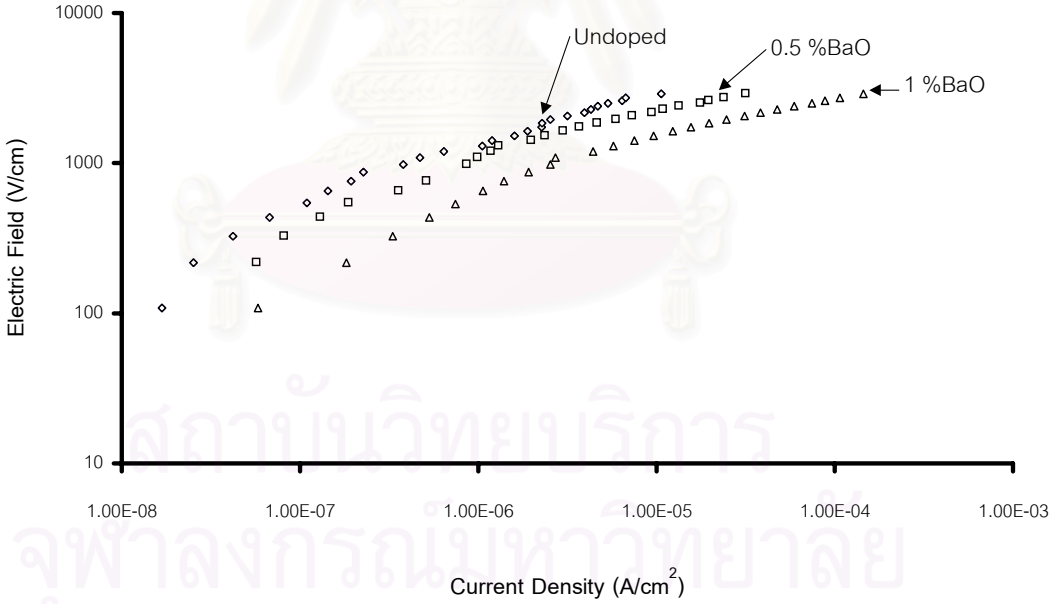

(II)

Figure 4.12 Current-voltage characteristics of doped and BaO-doped compositions sintered at 900°C for 2 hours in air (I : Linear scale ; II : Logarithmic scale).

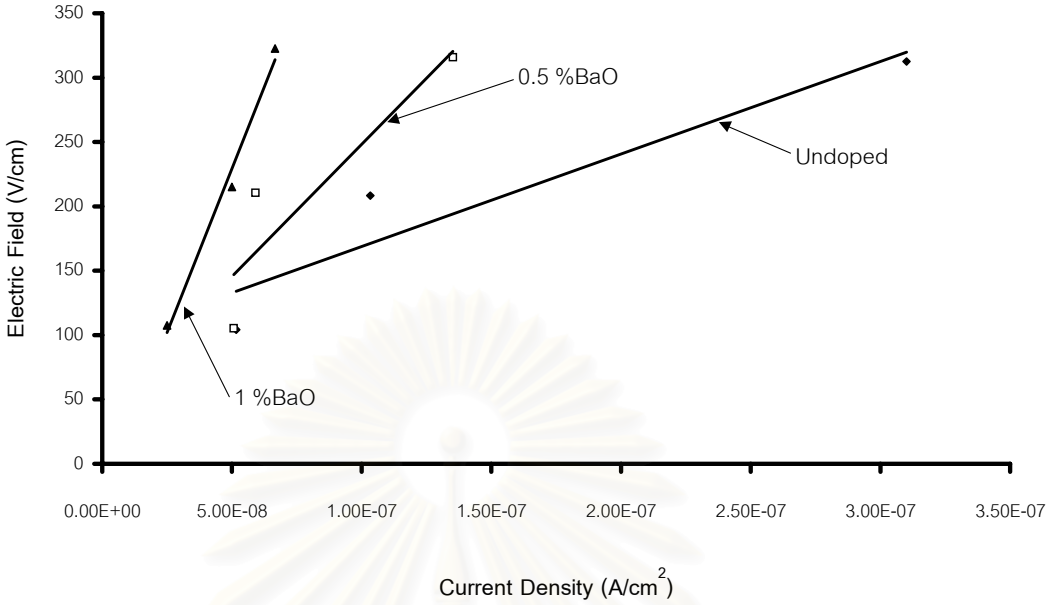

(I)

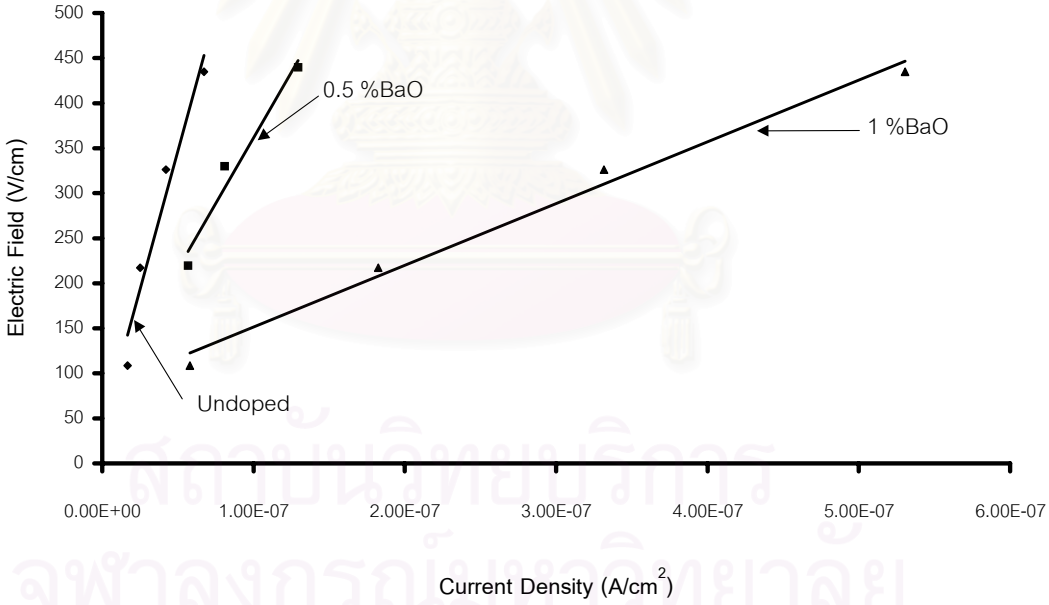

(II)

Figure 4.13 Linear current-voltage characteristics in prebreakdown region of samples sintered at 900°C for 2 hours (I : sintered in oxygen ; II : sintered in air).

4.3 Effect of Soaking Time

To study the effect of soaking time on the characteristics of varistor, 0.5 %BaO-doped base composition was sintered at 900 °C in oxygen with a different soaking period. Two and five-hour soaking times were selected in this investigation.

4.3.1 Crystal Phases

The results of X-ray diffraction patterns of the pellets sintered for 2 and 5 hours at 900 °C are displayed in Figure 4.14. Both results obtained are very similar, indicating that there is no phase change due to longer soaking time at this sintering temperature. The major and minor phases are previously identified to be the hexagonal ZnO and the bismuth-rich phases. Consequently, the phase formation is unaffected by changing the sintering soaking time from two to five hours.

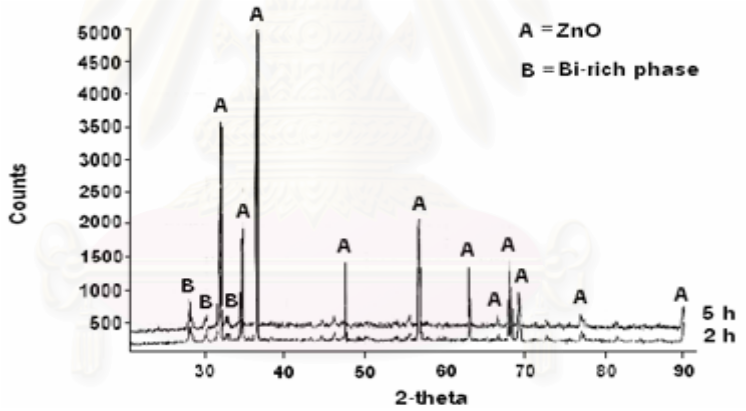

Figure 4.14 XRD patterns of 0.5% BaO-doped pellets sintered in oxygen at 900°C for 2 and 5 hours.

4.3.2 Microstructure

Figure 4.15 shows the SEM micrographs of 0.5 %BaO-doped composition sintered for 2 and 5 hours at 900 °C. It is found that the longer period of soaking time caused the nonuniform grain growth. This finding agrees with previous studies[27].

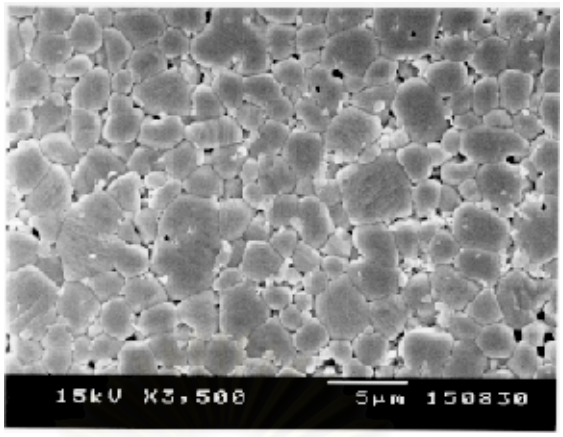

(I) 2 hours

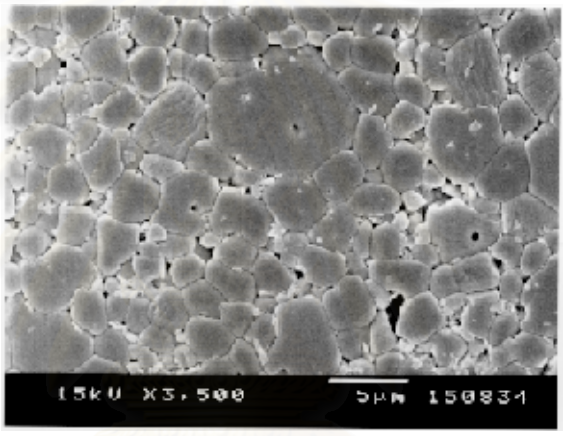

(II) 5 hours

Figure 4.15 SEM photomicrographs of 0.5% BaO-doped composition sintered at 900°C for 2 and 5 hours.

4.3.3 Current-Voltage (I-V) Characteristics

The I-V relation of the samples sintered for different period is presented in Figure 4.16. With increasing sintering time, the I-V curve is shifted down.

In prebreakdown region, the bulk resistivity decreases (from 3×10^{9} Ω.cm to 1×10^{9} Ω.cm) as the soaking time increases as observed from the slope of the

Figure 4.17. This may result from the larger grain size created by prolonging sintering time.

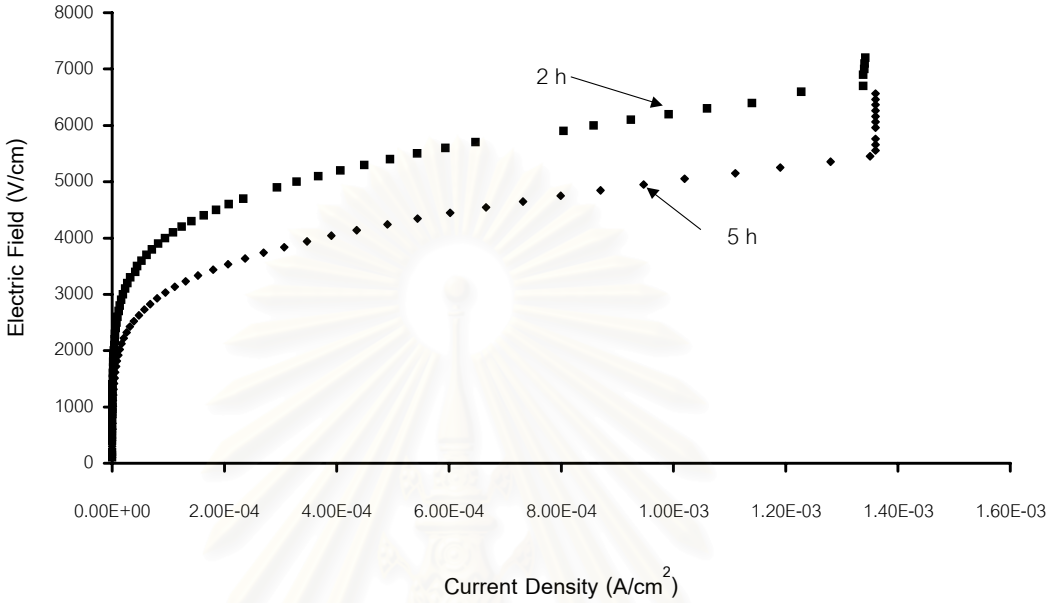

(I)

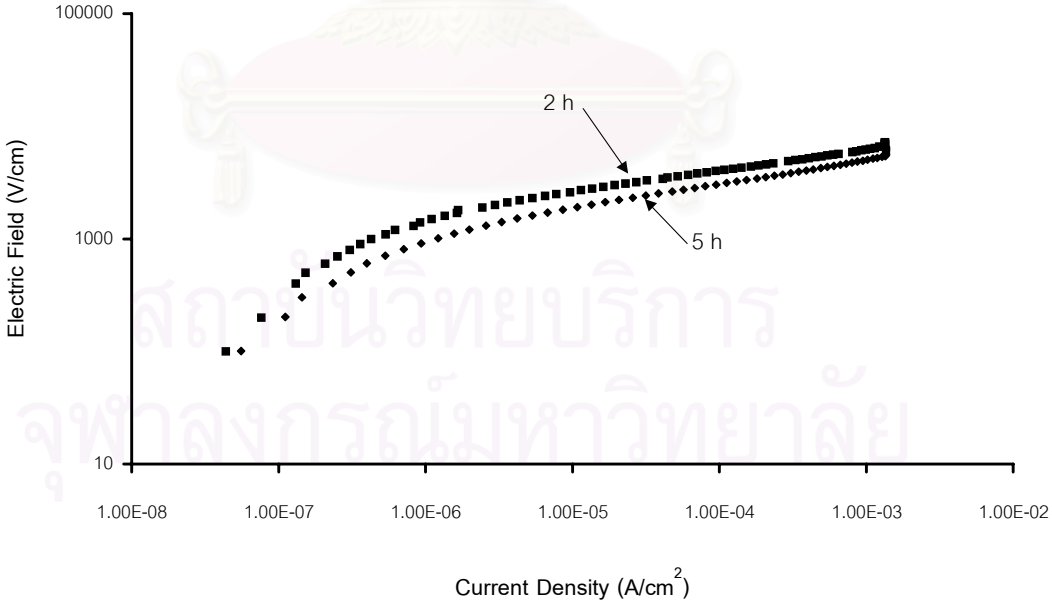

(II)

Figure 4.16 Current-voltage characteristic of 0.5% BaO-doped composition sintered at 900°C for 2 and 5 hours (I : Linear scale ; II : Logarithmic scale).

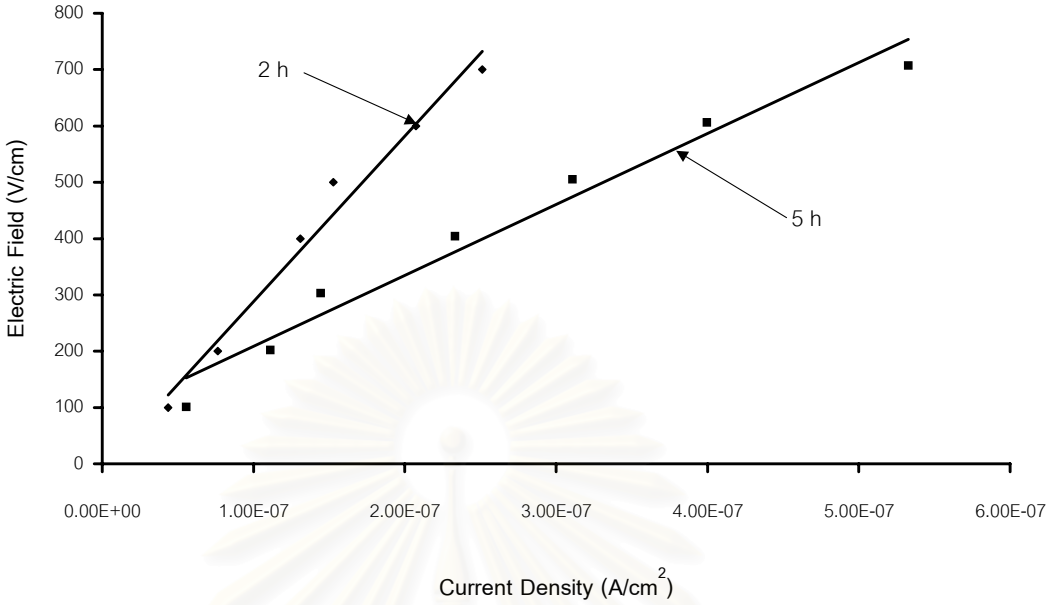

Figure 4.17 Linear current-voltage characteristic in prebreakdown region of 0.5% BaO-doped composition sintered at 900°C for 2 and 5 hours.

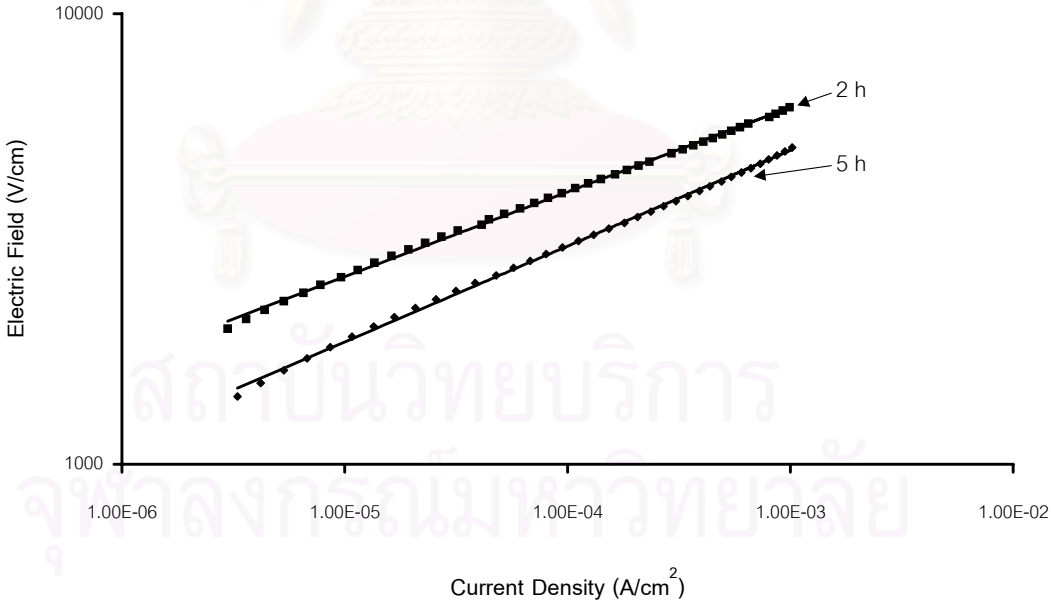

Figure 4.18 Nonlinear region of the current-voltage characteristics in nonlinear region of 0.5% BaO-doped composition sintered at 900°C for 2 and 5 hours.

In nonlinear region (Figure 4.18), the nonlinear coefficient (α) is likely reproduced in the sample sintered for 2 hours as previously reported. The coefficient (α) is slightly decreased when the soaking time raises from 2 to 5 hours. This may be due to an increase in grain size compensating with the nonuniform grain growth, which found in the sample sintered for longer period.

4.4 Effect of Sintering Temperature

4.4.1 Microstructure

Representative micrograph of the polished composition sintered at 1000 °C is shown in Figure 4.19. The higher sintering temperature yields more uniform microstructure as compared to that sintered at 900 °C on Figure 4.15. It should be noted that the magnifications used between Figures 4.15 and 4.19 are different.

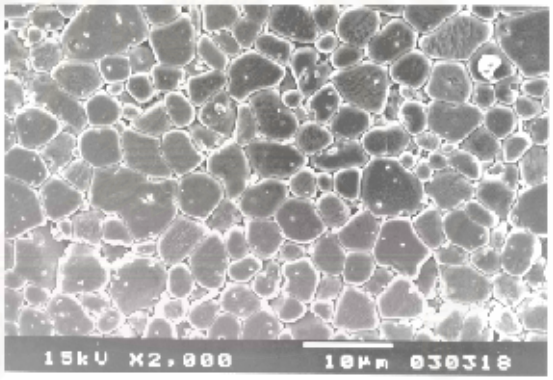

Figure 4.19 SEM photomicrograph of 0.5% BaO-doped composition sintered at 1000°C for 2 hours in oxygen.

4.4.2 Current-Voltage (I-V) Characteristics

Figure 4.20 shows the I-V curves of undoped and Ba-doped samples sintered at a higher sintering temperature of 1000 °C in oxygen. The undoped sample had the linear I-V behavior (α =1) while the 0.5 and 1.0 %BaO-doped samples still have the nonlinear I-V relation. The ohmic behavior in the undoped base composition occurs due to the lost of the Bi_2O_3 as discussed in the previous papers[26,32]. Since the nonohmic still appears in the 0.5 and 1.0 %BaO compositions sintered with the same condition, it implies that the BaO provides the stability of varistor performance. This can be confirmed by the presence of particles referred as the Bi-rich phases in previous part (4.2.1).

In prebreakdown region, BaO increasing gives rise in the bulk resistivity of the sample as presented in Table 4.4. This is also attributed to the stabilization of Bi_2O_3.

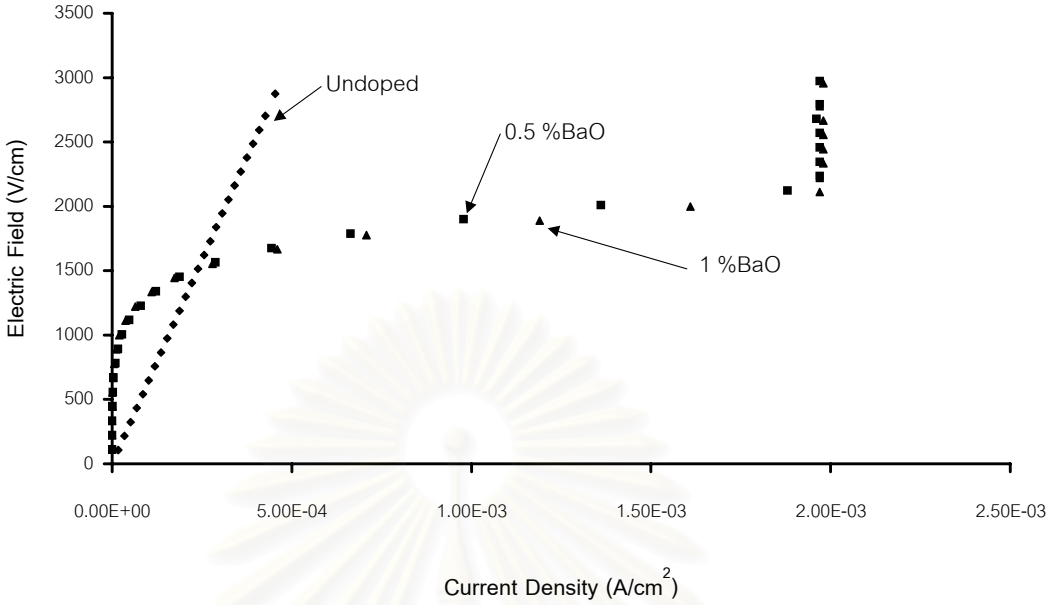

(I)

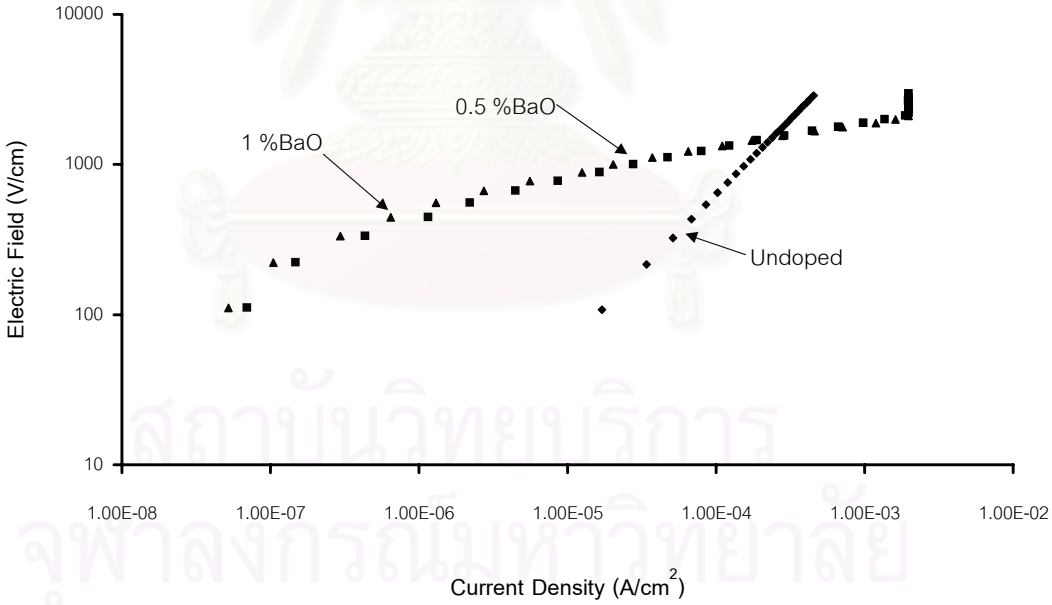

(II)

Figure 4.20 Current-voltage characteristics of undoped and BaO-doped compositions sintered at 1000°C for 2 hours in oxygen (I : Linear scale ; II : Logarithmic scale).

The nonlinear exponent increases as the BaO increases (Table 4.5). The maximum coefficient of about 7 is found in the 1 %BaO-doped sample. In addition, as compared to Table 4.3, the nonlinear coefficient increases when a higher sintering temperature of 1000 °C is applied. This result confirms that the higher α can be obtained from the sample sintered at a higher temperature resulting in the better uniform microstructure.

Table 4.4 Bulk resistivity as a function of %BaO additive of 95%ZnO-5%Bi_2O_3 sintered at 1000 °C for 2 hours in oxygen.

% BaO	Bulk Resistivity (Ω.cm)
0	0.06×10^8
0.5	1.00×10^8
1	2.00×10^8

Table 4.5 Nonlinear coefficient as a function of %BaO additive of 95%ZnO-5%Bi_2O_3 sintered at 1000 °C for 2 hours in oxygen.

% BaO	Nonlinear coefficient (α)
0	1
0.5	6.0
1	6.8

CHAPTER 5
SUMMARY, CONCLUSIONS AND SUGGESTION

5.1 Summary

In this thesis, the effects of BaO additive, sintering atmosphere, soaking time, and sintering temperature on the varistor characteristics of 95%ZnO-5%Bi_2O_3 ceramics were investigated.

5.1.1 Effect of BaO Dopant and Sintering Atmosphere

1. The crystal phases for all compositions sintered at 900 °C for 2 hours both in air and oxygen are the hexagonal ZnO (the major phase) and the bismuth-rich phases (the minor phases). This indicates that the formation of phases is independent of sintering atmosphere.

2. With BaO additive, the bulk density of 95%ZnO-5%Bi_2O_3 composition decreases. However, a higher density can be obtained in that sintered in oxygen. This confirms that the higher sintering temperature is required to achieve the optimum density.

3. The microstructure of these ceramics consists of ZnO grains, the particles of Bi-rich phases and pores. The grain size tends to grow with an addition of BaO and thus enhancing the numbers of pores.

4. The bulk resistivity depends on the BaO content and sintering atmosphere. With sintering in oxygen, the bulk resistivity increased as %BaO increases. Unlikely, the resistivity of samples sintered in air decreases as %BaO increases. It is possibly due to grain growth and oxygen vacancy or zinc interstitial taken place. Since BaO may prevent the loss of bismuth acted as the insulating barrier.

5. Both increasing in % BaO and sintering in oxygen bring about higher nonlinear coefficient (α). This may be due to the loss of Bi prevented by BaO additive.

5.1.2 Effect of Soaking Time

1. When soaking time increases from 2 to 5 hours, the phases detected by XRD are the same, which compose of the hexagonal ZnO and the Bi-rich phases. The independence of soaking time on the phases is identified.

2. The longer soaking time increases the grain size of composition.

3. The bulk resistivity decreases as the soaking time increases because of the larger grain size and the larger amount of Bi_2O_3 evaporated.

4. The nonlinear coefficient slightly decreases as prolong sintering. This results from an increase in grain size compensating with the nonuniform grain growth.

5.1.3 Effect of Sintering Temperature

1. The grain size of the samples sintered in oxygen for a constant soaking time of 2 hours increases as the sintering temperature increases.

2. Undoped composition sintered at 1000 °C in oxygen for 2 hours exhibits ohmic behavior because of the loss of Bi_2O_3 at high temperature. In contrast, Ba-doped compositions exhibit better nonlinear characteristics. This result indicates that BaO can stabilize Bi_2O_3 at higher sintering temperature. Moreover, the more uniformity of the microstructure also provides the better nonlinearity at higher sintering temperature.

3. The bulk resistivity decreases as the sintering temperature increases because of the loss of Bi_2O_3 insulating barrier and the larger in grain size.

5.2 Conclusions

1. BaO prevents the Bi_2O_3 evaporation and promotes the grain growth and a higher nonlinear coefficient.
2. Sintering in oxygen improves the nonlinear characteristics of varistor.
3. The increase in soaking time from two to five hours brings about the nonuniform grain growth, resulting in decreasing in nonlinear coefficient.
4. The increase in sintering temperature from 900 °C to 1000 °C also causes the more uniform grain growth bringing about a higher nonlinear coefficient.
5. The higher nonlinear coefficient is found in the sample having a larger grain size and a higher density. Furthermore, the better electrical property results from the uniform microstructure developed by increasing the sintering temperature.

5.3 Suggestion for Future Work

From this research, the density and the nonlinear coefficient are relatively low as compared to those from other works. To improve these characteristics, the following studies are suggested.

1. A study of varistor characteristics as a function of an amount of BaO with the higher sintering temperature.

2. A study of densification as a function of an amount of BaO with the higher sintering temperature.

3. A study of fabrication process of 95%ZnO-5%Bi_2O_3 ceramics with BaO additives.

4. A study of atomic defects of BaO-doped ZnO ceramics.

5. An application testing of BaO-doped ZnO ceramics at high current density with 8x20 μs waveshape.

REFERENCES

1. Clark, R. C. 1999. Varistor ceramics. J. Am. Ceram. Soc. 82 (3) : 485-502.

2. Wong, J. 1976. Barrier voltage measurement in metal oxide varistors. J. Appl. Phys. 47 (11) : 1827.

3. BrcÜknew, W. 1980. Inhomogenities and single barriers in ZnO varistor ceramics. Phys. Stat. Solid. (a) 59 (2) : 713.

4. Hozer, L. 1994. Semiconductor ceramics : Grain boundary effects. Warsaw : Polish Scientific Publishers PWN Ltd.

5. Emtage, P. R. 1979. Statistics and grain size in zinc oxide varistors. J. Appl. Phys. 50 (11) : 6833.

6. Philipp, H. R. and Levinson, L. M. 1979. High-temperature behavior of ZnO-base ceramic varistors. J. Appl. Phys. 50 (1) : 383.

7. Matsuoka, M. 1971. Nonohmic properties of zinc oxide ceramics. Jpn. J. Appl. Phys. 10 (6) : 736.

8. Mukae, K., Tsuda, K., and Nagasawa, I. 1977. Nonohmic properties of ZnO-rare earth metal oxide-Co_3O_4 ceramics. Jpn. J. Appl. Phys. 16 (8): 136.

9. William, P., Krivanek, O. L., and Thomans, G. 1980. Microstructure property relationships of rare-earth-zinc oxide varistors. J. Appl. Phys. 51 (7) : 3930.

10. Mukae, K. 1987. Zinc oxide varistors with praseodymium oxide. Ceram. Bull. 66 (9) : 1329.

11. Bhushan, B., Kashyap, S. C., and Chopra, K. L. 1981a. Novel nonohmic binary composite. Appl. Phys. Lett. 38 (3) : 160.

12. Bhushan, B., Kashyap, S. C., and Chopra, K. L. 1981b. Electrical and dielectric behavior of a zinc oxide composite. J. Appl. Phys. 52 (4) : 2932.

13. Carlson, W. G. and Gupta, T. K. 1982. Improve varistor nonlinearity via donor impurity doping. J. Appl. Phys. 53 (8) : 5746.

14. Gupta, T. K., Mathur, M. P., and Carlson, W. G. 1977. Effect of externally applied pressure on zinc oxide varistors. J. Electron Mater. 6 (5) : 483.

15. Levinson, L. M. and Philipp. 1976a. Ac properties of metal oxide varistors. J. Appl. Phys. 47 (3) : 1332.

16. Eda, K. 1989. Zinc varistor. IEEE Electrical Ins. Mag. 5 (6) : 28-41.

17. Gupta, T. K. 1990. Application of zinc oxide varistor. J. Am. Ceram. Soc. 73 (7) : 1817-1840.

18. Pike, G. E. 1994. Semiconducting Polycrystalline Ceramics. In M. V. Swain (ed.) Materials Science and Technology vol. 11. (Weinheim : Germany), pp. 731-754.

19. Einzinger, R. 1982. Grain boundary phenomena in ZnO varistor. In Leamy, H. J., Pike, G. E.,and Seager, C. H. (eds.) Grain boundaries in semiconductors (Elsevier : New York) : 343-355.

20. Levinson, L. M. and Philipp, H. R. 1975. The physics of metal oxide varistors. J. Appl. Phys. 46 (3) : 1332-1340.

21. Takemura, T., Kobayashi, Y., and Sato, K. 1986. Effects of bismuth sequioxide on the characteristics of ZnO varistors. J. Am. Ceram. Soc. 69 (5) : 430-436.

22. Olsson, E., Dunlop, G. L., and Österlund, R. 1989. Development of interfacial microstructure during cooling of a ZnO varistor material. J. Appl. Phys. 6 (10) : 5072-5077.

23. Medernach, O. W. and Synder, R. L. 1978. Powder diffraction patterns and structures of the bismuth oxides. J. Am. Ceram. Soc. 61 (11/12) : 494.

24. Levinson, L. M. and Philipp, H. R. 1986. Oxide varistors-A review. Ceram. Bull. 65 (4) : 639-646.

25. Levinson, L. M. and Philipp, H. R. 1991. Application and characterization of ZnO varistors. In Buchanan, R. C. (ed). Ceramic materials for electronics : processing properties, 2nd ed. (New York : Marcel Dekker, Inc.) : 350-377.

26. Asokan, T., Iyengar, G. N. K., and Nagabhushana, G. R. 1987. Influence of additive oxides on the electrical characteristics of ZnO-based composites. Br. Ceram. Trans. J. 86 : 190-193.

27. Fan, J and Freer, R. 1997. Varistor properties and microstructure of ZnO-BaO ceramics. J. Mat. Sci. 32 : 415-419.

28. Wong, J. 1974. Nature of intergranular phase in nonohmic ZnO ceramics containing 0.5% mol% Bi_2O_3. J. Am. Ceram. Soc. 57 (8) : 357-359.

29. Wong, J and Morris, W. G. 1974. Microstructure and phases in nonohmic ZnO-Bi_2O_3 ceramics. Ceram. Bull. 53 (11) : 816-820.

30. Inada, M. 1978. Crystal phases of nonohmic zinc oxide ceramics. Jpn. J. Appl. Phys. 17 (1) : 1-10.

31. Kim, D. D., Oh, M. H., and Kim, C. H. 1986. Effects of annealing on the grain boundary potential barrier of ZnO varistor. J. Mat. Sci. 21 (10) : 347-349.

32. Olsson, E., Österlund, R., and Dunlop, G. L. 1987. The role of interfacial microstructure of ZnO varistor materials. In Pask, J. A. and Evans, A. G. (eds), Ceramic microstructures '86 : Role of interfacial materials science research vol. 21 (New York : Plenum) : 679-686.

33. Asokan, T., Iyengar, G. N. K., and Nagabhushana, G. R. 1987. Studies on microstructure and density of sintered ZnO-based nonlinear resistors. J. Mat. Sci. 22 : 2229-2236.

34. Olsson, E. and Dunlop, G. L. 1989. Characteristic of individual interfacial in a ZnO varistor material. J. Appl. Phys. 63 (8) : 3666-3675.

APPENDICES

APPENDIX A

36-1451 Wavelength= 1.5405981

ZnO

Zinc Oxide

Zincite, syn

Rad.: CuKα1 λ: 1.5405 Filter: Graph Mono d-sp: Diffractometer

Cut off: 17.7 Int.: Diffract. I/Icor.:

Ref: McMurdie, H et al., Powder Diffraction, 1, 76 (1986)

Sys.: Hexagonal S.G.: $P6_3mc$ (186)

a: 3.24982(9) b: c: 5.20661(15 A: C: 1.6021

α: β: γ: Z: 2 mp:

Ref: Ibid.

Dx: 5.675 Dm: SS/FOM$_{25}$=131(.0071, 29)

εα: ηωβ: 2.013 εγ: 2.029 Sign+ 2V:

Ref: Dana's System of Mineralogy, 7th Ed., 1, 304

Color: Colorless

Peak height intensity. The approximate temperature of data collection was 26 C. References to other early patterns may be found in reference (5). The sample was obtained from the New Jersey Zinc Co., Bethlehem, PA, U/A. CAS #: 314-13-2. The structure was determined by Bragg (1) and refined by Abrahams, Berstein (2). $\sigma(I_{obs})$= ±1. A high pressure cubic NaCl-type of ZnO is reported by Bates et al. (3) and a cubic, sphalerite type is reported by Radczewski, Schicht (4). S Zn type, Wurtzite group, zincite subgroup. Also called: chinese white.PSC: hP4. To replace 3-664 (5). Mwt: 81.38. Volume[CD]: 47.62.

2θ	Int	h	k	l
31.770*	57	1	0	0
34.422*	44	0	0	2
36.253	100	1	0	1
47.539*	23	1	0	2
56.603*	32	1	1	0
62.864*	29	1	0	3
66.380*	4	2	0	0
67.963*	23	1	1	2
69.100*	11	2	0	1
72.562*	2	0	0	4
76.953*	4	2	0	2
81.370*	1	1	0	4
89.607*	7	2	0	3
92.784*	3	2	1	0
95.304*	6	2	1	1
98.613*	4	1	1	4
102.946	2	2	1	2
104.134	3	1	0	5
107.430	1	2	0	4
110.392	3	3	0	0
116.279	8	2	1	3
121.572	4	3	0	2
125.188	1	0	0	6
133.932	3	2	0	5
136.320	1	1	0	6
138.513	2	2	1	4
142.918	3	2	2	0

APPENDIX B

16-0654 Wavelength= 1.54434

δ-Bi2O3

Bismuth Oxide

Rad.: CuKα2 λ: 1.5443 Filter: d-sp:

Cut off: Int.: Estimation I/Icor.:

Ref: Gattow, Schroder, Z. Anorg. Allg. Chem., 318, 176 (1962)

Sys.: Cubic S.G.: Fm3m (225)

a: 5.66 b: c: A: C:

α: β: γ: Z: 2.4 mp:

Ref: Ibid.

Dx: 10.241 Dm: SS/FOM $_{15}$=7(.131, 13)

Pattern taken at 730 C. CAS #: 1304-76-3. Ca F2 type.
PSC: cF12. Mwt: 465.96. Volume[CD]: 181.32.

2θ	Int	h	k	l
27.317	100	1	1	1
31.668*	45	2	0	0
45.422*	65	2	2	0
53.688*	70	3	1	1
56.353*	18	2	2	2
65.883*	10	4	0	0
72.879*	23	3	3	1
74.891*	20	4	2	0
83.467*	18	4	2	2
90.217*	16	5	1	1
107.582	18	5	3	1
109.939	8	6	0	0

18-0244 Wavelength= 2.2909 O

β-Bi2O3

Bismuth Oxide

Rad.: CrKα λ: 2.2909 Filter: V Beta d-sp: Debye-Sheerrer

Cut off: Int.: Estimation I/Icor.:

Ref: Gattow, Schutze, Z. Anorg. Allg. Chem., 328, 44 (1964)

Sys.: Tetragonal S.G.: $P\bar{4}b2$ (117)

a: 10.93 b: c: 5.63 A: C: 0.5142

α: β: γ: Z: [8] mp:

Ref: Ibid.

Dx: 9.170 Dm: 9.231 SS/FOM $_{26}$=(.193,132)

CAS #: 1304-76-3. PSC: tP40. To replace 22-313. Mwt: 465.96. Volume[CD]: 673.05.

2θ	Int	h	k	l
36.999*	5			
42.790	100			
46.735*	5			
48.663*	20			
50.325*	30	3	2	1
64.554*	5	5	1	0
70.733*	5			
72.333*	40	4	4	0
73.341*	20	5	2	1
78.937*	5	6	1	0
81.208*	10	2	1	3
83.154*	5	2	2	3
83.971*	40			
88.603*	30	5	4	1
92.932*	30			
95.293*	5	5	5	0
96.112*	5			
101.420	5			
109.806	10	6	5	0
112.705	5	5	7	3
114.753	20	6	5	1
116.367	5	4	4	3
120.460	10	7	4	1
128.826	70	6	2	3
131.763	40	6	5	2
132.799	40	8	3	1
134.961	10	7	5	1
137.264	40	8	0	2
139.733	40	4	2	4
143.824	10			
148.796	10			
152.202	10	6	4	3

29-0236 Wavelength= 2.2909

β-Bi2O3

Bismuth Oxide

Rad.: CrKa λ: 2.2909 Filter: Beta d-sp:

Cut off: Int.: I/Icor.:

Ref: Correia Neves, J. et al., Rev. Cien. Geol. Ser. A., 7, 1 (1974)

Sys.: Tetragonal S.G.: $P\bar{4}b2$ (117)

a: 10.95 b: c: 5.63 A: C: 0.5142

α: β: γ: Z: mp:

Ref: Sillen, L., Ark. Mineral. Geol., 12A, 1 (1937)

Dx: Dm: $I//I_{cor}$=4(.061,121)

An intermediate phase of Bi2 O3 produced between 430-660 C. PSC: tP7. Mwt: 463.96. Volume[CD]: 673.03.

2θ	Int	h	k	l	2θ	Int	h	k	l
38.538*	20	3	1	0	132.382	60	4	0	4
42.087	100	2	2	1	134.318	40	7	3	1
43.729*	20	3	1	1	137.027	60	8	0	2
48.113*	40	0	0	2	138.476	60	8	4	0
49.339*	60	4	0	0					
63.266*	40	3	1	2					
69.642*	40	5	1	1					
71.323	100	4	0	2					
72.680*	60	4	1	2					
73.216*	40	0	0	3					
80.034*	40	5	3	1					
85.466	100	2	2	3					
87.662	100	6	2	1					
91.878*	60	4	4	2					
94.411*	40	5	3	2					
95.455*	20	4	0	3					
100.301	40	5	5	1					
108.883	40	0	0	4					
113.716	60	8	0	0					
115.283	40	5	5	2					
119.203	40	8	2	0					
128.451	100	6	2	3					
131.158	60	6	6	1					

41-1449 Wavelength= 1.34056

Bi2O3

Bismuth Oxide

Bismite, syn

Rad.: CuKα1λ: 1.3403 Filter: Quartz Monod-sp: Guinier 114.6

Cut off: Int.: Film I/Icor.: 1.4

Ref: Wies, S., Eysel, W., Mineral.-Petrograph. Inst., Univ. Heidelberg, Germany, ICDD Grant-in-Aid, (1989)

Sys.: Monoclinic S.G.: $P2_1/c$ (14)

a: 5.8499(3) b: 8.1698(4) c: 7.5123(3) A: 0.7160 C: 0.9193

α: β: 112.988(4) γ: Z: 4 mp:

Ref: Ibid.

Dx: 9.364 Dm: 8.640 SS/FOM$_{30}$=78(.0079, 49)

εα: ηωβ: =2.43 εγ: Sign: 2V:

Ref: Winchell, A., Winchell, H., Microscopic Character of Artificial Inorg. Solid Sub., 61 (1964)

Color: Light yellow

Pattern taken at 20 C. Sample from Ferak (puriss.mum).

Bi2 O3 (ypu. C.D. Cell: a=7.503, b=8.170, c=5.850, β=112.86, a/b=0.9187, c/b=0.7160, S.G.=P21/n(14). Silicon used as an internal stand. PSC: mP20. To replace 14-699 and alidated by calculated pattern 27-53. Mwt: 465.96. Volume[CD]: 330.52.

2θ	Int	h	k	l	2θ	Int	h	k	l
16.780*	1	0	1	1	47.576*	3	1	4	0
19.712*	2	1	1	1	48.397*	7	3	1	2
21.722*	3	0	2	0	48.397*	7	3	1	1
24.337*	1	1	0	2	48.576*	14	1	0	4
25.303*	<1	0	2	1	49.436*	7	1	3	3
25.737*	4	0	0	2	49.436*	7	1	3	2
26.922*	40	1	1	1	49.957*	1	1	1	3
27.377	100	1	2	0	50.391*	<1	2	0	2
28.000*	10	0	1	2	51.302*	3	1	4	2
32.484*	10	2	1	1	51.633*	2	2	1	4
33.039*	45	1	2	2	51.704*	9	2	1	2
33.039*	45	1	2	1	51.919*	8	0	3	3
33.241*	30	2	0	0	52.373*	45	3	2	1
33.941*	3	0	2	2	52.997*	11	2	3	1
35.042*	25	2	1	2	53.808*	<1	1	2	4
35.042*	25	2	1	0	54.169*	<1	0	1	4
35.406*	18	0	3	1	54.771*	12	2	4	1
35.906*	7	1	0	2	55.436*	10	2	2	4
36.962*	10	1	3	0	55.494*	10	2	2	2
37.593*	6	1	1	2	55.903*	3	3	2	0
40.053*	3	2	2	2	56.477*	1	2	4	2
40.624*	<1	0	1	3	57.754*	5	3	0	4
41.461*	5	1	3	1	57.866*	10	0	2	4
41.884*	4	2	1	3	57.941*	10	0	5	1
42.353*	18	1	2	2	58.266*	9	1	4	3
44.293*	2	0	4	0	58.363*	1	3	3	1
45.117*	14	0	2	3	58.969*	9	3	1	4
45.466*	1	2	3	1	59.032*	9	1	5	0
46.305*	45	0	4	1	59.032*	9	3	1	1
46.991*	2	3	0	2	59.891*	<1	1	3	4
47.431*	1	2	3	2	60.503*	<1	0	4	3
47.431*	1	2	3	0	61.488*	30	2	3	2

2θ	Int	h	k	l
61.488*	30	2	4	1
61.820*	10	3	3	3
62.291*	4	1	5	1
62.449*	3	1	0	4
62.343*	<1	3	2	1
62.849*	<1	0	5	2
63.433*	<1	2	1	5
63.559*	<1	4	0	2
63.693*	<1	0	3	4
64.707*	<1	4	1	2
65.373*	2	2	5	1
66.264*	3	4	1	1
66.393*	2	1	4	2
66.393*	2	1	4	1
66.810*	5	2	2	3
66.902*	7	2	5	2
67.463*	<1	3	0	2
67.870*	<1	1	4	3
68.140*	<1	3	3	1
68.371*	2	3	1	2
68.789*	<1	0	1	5
68.916*	2	0	6	0
69.276*	1	2	4	4
69.563*	2	4	2	1
69.632*	5	3	4	3
69.800*	<1	4	0	0
70.417*	<1	0	6	1
70.606*	1	0	5	3
70.793*	<1	4	1	4
70.861*	3	4	1	0
71.388*	6	1	6	1
71.482*	<1	2	5	3
71.482*	<1	2	5	1
72.030*	2	0	2	5
72.318*	3	2	3	3
72.393*	<1	1	3	4
73.427*	1	4	3	2
74.029*	2	4	2	4
74.382*	2	1	6	1
74.918*	2	4	3	1
75.398*	<1	3	4	4
76.103*	<1	2	0	4

45-1344 Wavelength= 1.5405981

γ-Bi2O3

Bismuth Oxide

Rad.: CuKα1 λ: 1.5405 Filter: Ge Mono d-sp: Diffractometer

Cut off: Int.: Diffract. I/Icor.: 4.7

Ref: Wies, S., Eysel, W., Mineral.-Petrographisches Inst., Univ. Heidelberg, Germany, ICDD Grant-in-Aid, (1991)

Sys.: Cubic S.G.: I23 (197)

a: 10.2670(2) b: c: A: C:

α: β: γ: Z: 13 mp:

Ref: Harvig, H., Z. Anorg. Allg. Chem., 444, 151 (1978)

Dx: 9.294 Dm: SS/FOM $_{31}$=160(.0049, 38)

Color: Greenish yellow

Prepared by Bi2 O3 (Aldrich, 99.999%) heated in a sealed Au tube to 850 C, cooled with 2 K per minute to 630 C and quenched in liquid N2. Lattice parameter in good agreement with the value 10.268, given by Levin, Roth, J. Res. Nat. Bur. Stand., Sect. A, 68 189-195 (1984). Metastable phase. Bi2 O3 type. Silicon used as an internal stand. PSC: cI65. Mwt: 465.96. Volume[CD]: 1082.26.

2θ	Int	h	k	l	2θ	Int	h	k	l
17.252*	2	2	0	0	83.000*	1	7	5	2
21.182*	2	2	1	1	84.278*	1	8	4	0
24.310*	12	2	2	0	85.593*	2	8	3	3
27.455*	100	3	1	0	86.878*	3	8	4	2
30.124*	40	2	2	2	88.179*	3	7	6	1
32.607*	80	3	2	1	89.454*	2	6	6	4
34.926*	3	4	0	0					
37.126*	4	3	3	0					
39.214*	8	4	2	0					
41.203*	20	3	3	2					
43.128*	16	4	2	2					
44.981*	18	4	3	1					
48.325*	2	5	2	1					
51.888*	50	4	3	3					
53.510*	12	4	4	2					
55.094*	25	5	3	2					
59.697*	2	6	2	2					
61.179*	25	6	3	1					
64.080*	9	5	4	3					
65.511*	4	6	4	0					
66.926*	4	7	2	1					
68.311*	1	6	4	2					
69.695*	1	7	3	0					
72.429*	2	7	3	2					
75.129*	1	5	5	4					
77.775*	10	6	5	3					
79.071*	9	8	2	2					
80.393*	8	7	5	0					

37-0054 Wavelength= 1.54050 C

BiO

Bismuth Oxide

Rad.: CuKα1 λ: 1.5405 Filter: d-sp: Calculated

Cut off: Int.: Calculated I/Icor.:

Ref: Medernach, J., Snyder, N.Y.S. College of Ceramics, Alfred Univ., Alfred, New York, USA, ICDD Grant-in-Aid

Sys.: Rhombohedral S.G.: R3m (160)

a: 3.88 b: c: 9.710 A: C: 2.5026

α: β: γ: Z: 3 mp:

Ref: Ibid.

Dx: 8.833 Dm: SS/FOM $_{30}$=396(.0025, 30)

Peak height intensity. Bi O type. PSC: hR2. Mwt: 224.98. Volume[CD]: 126.59.

2θ	Int	h	k	l	2θ	Int	h	k	l
27.331*	40	0	0	3	103.045	1	2	0	8
28.080	100	1	0	1	105.135	1	2	2	0
32.374*	56	0	1	2	109.550	2	1	1	9
46.089*	23	1	0	4	110.632	2	2	1	7
46.786*	23	1	1	0	111.327	1	1	0	10
54.579*	10	0	1	5	111.980	3	2	2	3
55.148*	24	1	1	3	112.255	3	1	3	1
55.473*	12	0	2	1	113.507	2	3	0	0
56.844*	3	0	0	6	114.623	2	3	1	2
58.043*	8	2	0	2	122.751	2	1	2	8
67.773*	5	0	2	4	124.388	2	1	3	4
73.844*	4	1	0	7	128.883	1	0	1	11
74.637*	3	2	0	5	132.754	2	0	2	10
75.418*	7	2	1	1	133.958	1	4	0	1
76.606*	6	1	1	6	135.373	2	2	2	6
77.641*	5	1	2	2	137.054	1	0	4	2
84.863*	2	0	1	8	151.960	1	4	0	4
86.390*	4	2	1	4	160.619	1	2	0	11
86.891*	2	3	0	0	164.883	2	3	0	9
91.110*	1	0	0	9					
92.119*	2	0	2	7					
92.883*	3	1	2	5					
93.385*	4	3	0	3					

26-0230 Wavelength= 1.54056

Bi48ZnO73

Zinc Bismuth Oxide

Rad.: Cu λ: 1.5405 Filter: d-sp:

Cut off: Int.: Estimation I/Icor.:

Ref: Safronov et al., Russ. J. Inorg. Chem. (Engl. Transl.), 16, 460 (1971)

Sys.: Cubic S.G.:

a: 10.20 b: c: A: C:

α: β: γ: Z: mp: 730

Ref: Ibid.

Dx: Dm: SS/FOM$_{25}$=6(.072, 63)

Possible silleniite type structure such as Bi12 Ge O20. Mwt: 11264.39. Volume[CD]: 1061.32.

2θ	Int	h	k	l	2θ	Int	h	k	l
21.290*	2	2	1	1	72.933*	6	6	5	1
24.710*	20	2	2	0	75.796*	2	7	4	1
27.681	100	3	1	0	77.101*	1	8	2	0
30.272*	25	2	2	2	78.380*	30	6	5	3
32.815*	80	3	2	1	79.708*	25	6	6	0
35.178*	6	4	0	0	80.922*	20	7	5	0
37.264*	10	3	3	0					
39.401*	10	4	2	0					
41.463*	20	3	3	2					
43.362*	20	4	2	2					
45.237*	25	5	1	0					
48.402*	6	5	2	0					
52.164*	40	5	3	0					
53.852*	20	6	0	0					
55.439*	30	6	1	1					
58.559*	2	5	4	1					
60.153*	2	6	2	2					
61.569*	20	6	3	1					
63.588*	2	7	0	0					
64.526*	9	5	5	0					
67.360*	4	7	2	1					
69.522*	4	7	2	2					
70.661*	4	7	3	1					

41-0253 Wavelength= 1.54056

ZnBi38O60

Zinc Bismuth Oxide

Rad.: CuKα1 λ: 1.5405 Filter: Quartz Monod-sp: Guinier

Cut off: Int.: Diffract. I/Icor.: 1.04

Ref: Tomala, Kyasl, Mineralogisch-Petrographisches Institut der Universitaet Heidelberg, Germany, ICDD Grant-in-Aid, (1989)

Sys.: Cubic S.G.: I23 (197)

a: 10.2049(2) b: c: A: C:

α: β: γ: Z: 0.667 mp:

Ref: Ibid.

Dx: 9.345 Dm: SS/FOM$_{30}$=133(.0073, 31)

Color: Yellowish gray

Stoichiometric mixture of Bi2 O3 (Ventron, ultrapure) and ZnO (Ventron, purisa.) annealed in an open Au-crucible at 750 C for 3 weeks with several intermediate grindings. This compound contains some Bi +5; therefore the formula is Zn Bi36 +3 Bi2O60 +5. The formula Bi48 Zn O73 reported for this compound by Safronov et al., Russ. J. Inorg. Chem., 16 460 (1971) is wrong. Silleniite, Bi12 O20 Si type. Silicon used as an internal stand. PSC: cI66.03. Mwt: 8966.80. Volume[CD]: 1062.74.

2θ	Int	h	k	l	2θ	Int	h	k	l
17.377*	1	2	0	0	76.998*	1	6	4	4
21.303*	3	2	1	1	78.327*	12	6	5	3
24.654*	16	2	2	0	79.652*	12	6	6	0
27.628	100	3	1	0	80.988*	12	7	4	3
30.325*	25	2	2	2	82.298*	<1	6	6	2
32.815*	75	3	2	1	83.605*	3	7	5	2
35.150*	4	4	0	0	84.932*	1	8	4	0
37.370*	5	3	3	0	86.242*	3	9	1	0
39.456*	7	4	2	0	87.520*	4	8	4	2
41.469*	12	3	3	2	88.834*	6	6	5	5
43.408*	12	4	2	2	90.162*	1	6	6	4
45.269*	14	4	3	1					
48.853*	6	5	2	1					
50.541*	<1	4	4	0					
52.225*	30	4	3	3					
53.859*	16	4	4	2					
55.454*	25	5	3	2					
57.047*	1	6	2	0					
58.563*	3	5	4	1					
60.089*	3	6	2	2					
61.583*	18	6	3	1					
63.077*	2	4	4	4					
64.511*	9	5	4	3					
65.958*	2	6	4	0					
67.371*	5	7	2	1					
68.818*	2	6	4	2					
70.182*	2	7	3	0					
72.933*	3	6	5	1					
74.280*	<1	8	0	0					
75.640*	3	7	4	1					

42-0183 Wavelength= 1.5406

Bi3RZnO8

Zinc Bismuth Oxide

Rad.: CuKα1 λ: 1.5406 Filter: Ni Beta M d-sp: Diffractometer

Cut off: Int.: Diffract. I/Icor.: 3.0

Ref: Troemel, M., Dellicat, U., Duecke, J., Muench, L., Inst. Anorg. Chem., Frankfurt, Germany, ICDD Grant-in-Aid, (1991)

Sys.: Cubic S.G.: I23 (197)

a: 10.206 b: c: A: C:

α: β: γ: Z: 0.666 mp:

Ref: Craig, D., Stephenson, N., J. Solid State Chem., 15, 1 (1975)

Dx: 9.295 Dm: SS/FOM$_{31}$=74(.0135, 30)

Color: Light yellow

Prepared by heating oxides at 750 C for 3 weeks. 26 metal atoms per cell. Sillenite, Bi12 O20 Si type. Also called: γ*-\Bi2 O3\,PSC: cI64.60, Mwt: 8934.60, Volume[CD]: 1063.08.

2θ	Int	h	k	l	2θ	Int	h	k	l
12.249*	<1	1	1	0	67.362*	7	5	5	2
17.340*	1	2	0	0	68.768*	3	6	4	2
21.290*	3	2	1	1	70.178*	2	7	3	0
24.655*	20	2	2	0	72.935*	7	6	5	1
27.611*	100	3	1	0	74.268*	1	8	0	0
30.304*	26	2	2	2	75.656*	5	7	4	1
32.828*	89	3	2	1	76.956*	2	8	2	0
35.137*	4	4	0	0	78.306*	19	6	5	3
37.361*	7	4	1	1	79.631*	19	8	2	2
39.436*	10	4	2	0	80.966*	17	7	5	0
41.484*	14	3	3	2	82.309*	1	6	6	2
43.407*	15	4	2	2	83.598*	4	7	5	2
45.287*	22	5	1	0	84.925*	1	8	4	0
48.846*	7	5	2	1	86.275*	6	9	1	0
50.534*	1	4	4	0	87.543*	6	8	4	2
52.198*	47	5	3	0	88.837*	9	9	2	1
53.898*	23	4	4	2	90.155*	1	6	6	4
55.477*	37	5	3	2	91.455*	8	9	3	0
57.052*	1	6	2	0	94.065*	3	9	3	2
58.560*	4	5	4	1	95.396*	1	8	4	4
60.069*	4	6	2	2	96.711*	17	9	4	1
61.571*	29	6	3	1	97.995*	2	10	0	0
63.060*	2	4	4	4	99.321*	1	10	1	1
64.528*	13	5	4	3	100.631	3	10	2	0
65.912*	3	6	4	0	101.984	7	9	4	3

2θ	Int	h	k	l
103.334	3	10	2	2
104.685	8	10	3	1
107.382	3	8	5	3
108.777	2	10	4	0

43-0449 Wavelength= 1.5406

Bi7.65Zn0.35O11.83

Zinc Bismuth Oxide

Rad.: CuKα1 λ: 1.5406 Filter: Ni Beta M d-sp: Diffractometer

Cut off: Int.: Diffract. I/Icor.:

Ref: Troemel, M., Dellicat, U., Muench, B., Institut für Anorganische Chemie, Frankfurt, Germany, ICDD Grant-in-Aid, (1992)

Sys.: Tetragonal S.G.: $I\bar{4}2_1c$ (114)

a: 7.7283(3) b: c: 8.6406(4) A: C: 0.7299

α: β: γ: Z: 1 mp:

Ref: Ibid.

Dx: 8.926 Dm: SS/FOM$_{31}$=22(.0147, 93)

Color: Orange

Prepared by melting mixtures of Bi2 O3 and ZnO at 1000 C for 2 minutes and quenching in ice-water. β-Bi2 O3 type. Also called: β*-\Bi2 O3\,PSC: tI19.83, Mwt: 1810.86, Volume[CD]: 336.89.

2θ	Int	h	k	l	2θ	Int	h	k	l
16.191*	1	1	1	0	73.656*	5	6	0	1
27.936	100	2	0	1	75.870*	9	2	2	4
31.693*	18	0	0	2	77.550*	7	4	4	2
32.741*	23	2	2	0	78.153*	8	6	2	0
38.071*	1	3	0	1	78.153*	8	3	1	4
40.190*	<1	3	1	1	83.100*	6	4	0	4
41.256*	1	2	1	2	86.782*	11	6	2	2
43.235*	1	3	2	1	90.665*	4	5	3	3
46.234*	39	2	2	2	90.665*	4	2	0	5
47.020*	13	4	0	0	91.828*	<1	5	1	5
49.298*	<1	3	1	2	92.924*	4	6	0	3
49.843*	1	4	0	1	94.033*	7	6	4	1
49.843*	1	1	0	3	94.033*	7	6	1	3
53.649*	1	3	2	2	103.452	4	4	4	4
54.198*	23	2	0	3	105.783	2	8	0	0
55.587*	34	4	2	1	105.783	2	5	3	4
55.587*	34	2	1	3					
57.796*	14	4	0	2					
66.229*	2	0	0	4					
67.473*	<1	1	0	4					
68.653*	5	4	4	0					
68.653*	5	1	1	4					
71.092*	<1	5	3	0					
71.092*	<1	2	0	4					
74.341*	14	4	2	3					

BIOGRAPHY

Miss Chiraporn Auechalitanukul was born on December 20, 1976 in Bangkok. She received a bachelor degree in material science from Faculty of Science, Chulalongkorn University in 1998. She continued a further study in Master Degree in the field of Ceramic Technology at the same place in June 1998 and completed all of programs in October 2000.